

**Mixed NNLO QCD  $\times$  electroweak corrections  
to single-Z production in pole approximation:  
differential distributions and forward–backward asymmetry**

STEFAN DITTMAYER<sup>1</sup>, ALEXANDER HUSS<sup>2</sup> AND JAN SCHWARZ<sup>1</sup>

<sup>1</sup> *Albert-Ludwigs-Universität Freiburg, Physikalisches Institut,  
Hermann-Herder-Straße 3, D-79104 Freiburg, Germany*

<sup>2</sup> *Theoretical Physics Department, CERN, 1211 Geneva 23, Switzerland*

**Abstract:**

Radiative corrections in pole approximation, which are based on the leading contribution in a systematic expansion of amplitudes about resonance poles, naturally decompose into *factorizable* corrections attributed to the production or decay of the resonance and *non-factorizable* corrections induced by soft photon (or gluon) exchange between those subprocesses. In this paper we complete an earlier calculation of mixed QCD  $\times$  electroweak corrections of  $\mathcal{O}(\alpha_s\alpha)$  to the neutral-current Drell–Yan cross section in pole approximation by including the previously neglected corrections that are solely related to the Z-boson production process. We present numerical results both for differential distributions and for the forward–backward asymmetry differential in the lepton-pair invariant mass, which is the key observable in the measurement of the effective weak mixing angle at the LHC. Carefully disentangling the various types of factorizable and non-factorizable corrections, we find (as expected in our earlier work) that the by far most important contribution at  $\mathcal{O}(\alpha_s\alpha)$  originates from the interplay of initial-state QCD corrections and electroweak final-state corrections.

January 2024

## 1 Introduction

Owing to its large cross section and clean experimental signature, the Drell–Yan-like production of charged leptons is among the most important standard-candle processes at hadron colliders such as the Tevatron and the LHC [1–4]. The charged-current channel (W production) allows for the determination of the mass and width of the W boson [5–9], the neutral-current channel (Z production) for the measurement of the effective weak mixing angle [5, 10–14], both with extraordinary precision. For these high-precision measurements, among the most relevant observables are the transverse-momentum and invariant-mass distributions, as well as the differential forward–backward asymmetry of the charged lepton pair from Z production, in the vicinity of the W- and Z-boson resonances. Moreover, Drell–Yan cross sections significantly contribute to the determination of the parton distribution functions (PDFs) via rapidity distributions and the W-boson charge asymmetry [15]. Last but not least, Drell–Yan-like processes are well suited to search for new  $W'$  and  $Z'$  bosons in the high invariant-mass range of the final-state leptons.

All these measurements and precision tests of the Standard Model require precise predictions for differential Drell–Yan cross sections at the highest possible level in order to match or better surpass the experimental uncertainties. To this end, radiative corrections of the strong and electroweak (EW) interactions as well as corrections mixing these types of interactions have to be calculated to higher orders in perturbation theory. Fixed-order QCD calculations are available fully differentially at next-to-next-to-leading order (NNLO) [16–23] with third-order results ( $N^3$ LO) known fully inclusively [24–26], single-differentially [27, 28], and at the fiducial level [28–30]. Additionally, the resummation of large QCD logarithms occurring due to soft-gluon emissions at small transverse momentum has been studied in Refs. [30–43], and threshold effects have been calculated up to  $N^3$ LO in QCD [44, 45]. On the EW side, the next-to-leading order (NLO) corrections are known [46–61] as well as leading higher-order effects from multiple photon emissions or of universal origin [54, 56, 57, 62, 63].

The mixing of QCD and EW corrections begins at NNLO, i.e. at  $\mathcal{O}(\alpha_s\alpha)$ . The calculation of these corrections to W and Z production started in Refs. [64, 65] in pole approximation (PA), which is based on the leading contribution in an expansion of all matrix elements about the resonance poles (see, e.g., Ref. [66] for the general concept). The PA reduces the complexity of the loop calculations, e.g. by avoiding two-loop box diagrams with the full  $2 \rightarrow 2$  kinematics, and classifies the  $\mathcal{O}(\alpha_s\alpha)$  corrections into four separately gauge-invariant contributions [64]: (i) *factorizable initial–final (IF) corrections* including QCD corrections to W/Z production and EW corrections to the W/Z decay, (ii) *factorizable initial–initial (II) corrections* including mixed NNLO QCD  $\times$  EW corrections to on-shell W/Z production, (iii) *final–final (FF) corrections* with QCD and EW corrections confined in the W/Z decays, and (iv) *non-factorizable (NF) corrections* linking the QCD-corrected W/Z production to the leading-order (LO) decay process by soft photon exchange or emission. The NF and FF corrections have been calculated in Ref. [64] and Ref. [65], respectively, and found to be insignificant in differential cross sections. The corrections of type IF have been evaluated in Ref. [65] as well and found to be sizeable owing to the interplay of the large QCD corrections in the production with enhanced

photonic final-state radiation effects. These corrections, in particular, induce a shift in the  $W$ -boson mass extracted from the charged-current process which was estimated to be about 10 MeV. The II corrections had been neglected in Refs. [64, 65], following arguments that they are expected to be subleading wrt. the IF corrections owing to the absorption of the enhanced collinear ISR effects into the PDFs in contrast to the situation for FSR. The missing II corrections of  $\mathcal{O}(\alpha_s\alpha)$  meanwhile have been calculated in Refs. [67] and [68–75] for  $W$  and  $Z$  production, but unfortunately have not yet been combined with the other correction types to a full prediction in PA.

More recently, the  $\mathcal{O}(\alpha_s\alpha)$  corrections to the full off-shell Drell–Yan processes have been attacked by several groups, starting with the  $\mathcal{O}(N_f\alpha_s\alpha)$  corrections to the charged- and neutral-current channels which are enhanced by the number  $N_f$  of fermion flavours [76]. For the off-shell charged-current process, the  $\mathcal{O}(\alpha_s\alpha)$  corrections have been evaluated in approximate form, taking into account real and real–virtual NNLO corrections exactly, but neglecting the genuine two-loop corrections [77]. For the off-shell neutral-current process, the full  $\mathcal{O}(\alpha_s\alpha)$  corrections have been calculated by two groups [78–80]. While these achievements can certainly be considered as a major breakthrough in the calculation of mixed QCD  $\times$  EW corrections to  $2 \rightarrow 2$  scattering processes, we still see the need to complete the discussion of the phenomenological structure and impact of the  $\mathcal{O}(\alpha_s\alpha)$  corrections to Drell–Yan processes at least in two respects. Firstly, a thorough comparison of the approximate and full off-shell calculations with PA predictions is very desirable, to better understand the origin of the dominant effects and to obtain further guidance in the construction of approximations that are numerically more efficient to evaluate. Secondly, for the neutral-current case a proper phenomenological discussion of the  $\mathcal{O}(\alpha_s\alpha)$  corrections to the differential forward–backward asymmetry still does not exist in the literature.

In this paper we prepare for the first aspect by completing the PA prediction started in Refs. [64, 65] by calculating the missing II corrections to  $Z$  production. Since Ref. [78] employs the same setup as already used in our previous calculation [64, 65], we keep this setup in this paper as well and compare our PA results on differential cross sections with the results from the off-shell calculation of Ref. [78], which are based on bare muons. A more complete comparison, including results based on dressed leptons as used in Ref. [79], is beyond the scope of this paper and will certainly be carried out within the LHC Electroweak Working Group in the near future. The major part of our discussion of numerical results is devoted to the  $\mathcal{O}(\alpha_s\alpha)$  corrections to the forward–backward asymmetry in the  $Z$  resonance region in the neutral-current Drell–Yan process. This discussion is of particular relevance for the theory predictions to the experimental determination of the effective weak mixing angle at the LHC.

This paper is organized as follows: In Section 2 we give a short overview of the gauge-invariant PA contributions to the  $\mathcal{O}(\alpha_s\alpha)$  corrections and discuss our calculation of contributions of type II. The latter are divided into mixed QCD  $\times$  weak and QCD  $\times$  photonic corrections in a gauge-invariant way on the basis of selecting appropriate subsets of diagrams. The QCD  $\times$  weak part comprises only genuine two-loop corrections to the  $Z\bar{f}f$  vertex and real–virtual corrections with jet emission. Our result for the corresponding two-loop formfactor, which was first calculated in Ref. [81], is presented in App. A. Since the infrared (IR) singularities in the QCD  $\times$  weak corrections are only of NLO complexity,

we apply both the antenna [82] and dipole subtraction [83] approaches to combine the two IR-singular parts to a total IR-finite result. The QCD  $\times$  photonic corrections feature double-virtual, real-virtual, and double-real corrections. To isolate and combine all NNLO IR singularities, which is the major complication in this part, we apply antenna subtraction as introduced in Refs. [84, 85]. Our calculation is the first application of antenna subtraction to  $\mathcal{O}(\alpha_s\alpha)$  corrections. In Section 3 we present a detailed discussion of the  $\mathcal{O}(\alpha_s\alpha)$  corrections to neutral-current DY processes in the Z-resonance region on various distributions, with special emphasis on the newly calculated corrections to the forward-backward asymmetry. To complete the phenomenological picture we also provide full NLO results (i.e. without resorting to the PA), split into a genuine weak part and photonic parts induced by initial-state radiation, final-state radiation, and initial-final interference. The PA-based  $\mathcal{O}(\alpha_s\alpha)$  correction is split into II, FF, IF, and NF parts as introduced above. Finally, we also evaluate the relevant leading EW effects beyond NNLO, which are induced by multi-photon radiation and the leading universal EW renormalization effects. Our summary is given in Section 4, and the appendices provide further analytical results.

## 2 Details of the calculation

In this section we describe the calculation of  $\mathcal{O}(\alpha_s\alpha)$  corrections to the neutral-current Drell-Yan process in PA. In Section 2.1 we give an overview of the separately gauge-invariant building blocks of the PA at  $\mathcal{O}(\alpha_s\alpha)$ . Corrections of initial-initial type—i.e. the  $\mathcal{O}(\alpha_s\alpha)$  corrections with both QCD and EW corrections to the production of the Z boson—are the last missing piece to complete the calculation [64, 65] of  $\mathcal{O}(\alpha_s\alpha)$  corrections to DY-like Z-boson production in PA; their calculation is described in Section 2.2.

### 2.1 $\mathcal{O}(\alpha_s\alpha)$ corrections to single-Z production in pole approximation

The expansion of the full NNLO  $\mathcal{O}(\alpha_s\alpha)$  correction around the Z resonance pole at  $p_Z^2 \approx M_Z^2$  leads to the following four types of corrections [64, 65], which are illustrated for the purely virtual two-loop corrections in Fig. 1:

- Factorizable  $\mathcal{O}(\alpha_s\alpha)$  corrections of initial-final (IF) type combine the  $\mathcal{O}(\alpha_s)$  corrections to Z production and the  $\mathcal{O}(\alpha)$  correction to the leptonic Z decay. Here and in the following the terminology “factorizable” refers to the fact that the corresponding amplitudes all factorize in terms of subamplitudes for production and decay and a resonant Z-boson propagator. The strong collinear enhancement of final-state photon radiation renders the IF class of  $\mathcal{O}(\alpha_s\alpha)$  corrections by far the dominant PA contribution in the resonance region [65].
- The factorizable initial-initial (II)  $\mathcal{O}(\alpha_s\alpha)$  corrections contain contributions where both QCD and EW corrections are located in the Z-boson production subprocess. This contribution is essentially furnished by the corrections to on-shell Z production, supplemented by the off-shell Z propagator and the leptonic Z decay in LO. Since both QCD and photonic effects from initial-state radiation are widely absorbed into PDFs, the type-II  $\mathcal{O}(\alpha_s\alpha)$  corrections were expected to be suppressed wrt. to the dominating IF corrections and neglected in Refs. [64, 65]. In this paper, we

complete the PA at  $\mathcal{O}(\alpha_s\alpha)$  by supplementing the corrections of type II. We split the II corrections into the separately gauge-invariant QCD $\times$ weak and QCD $\times$ photonic parts of the orders  $\mathcal{O}(\alpha_s\alpha_w)$  and  $\mathcal{O}(\alpha_s\alpha_p)$ , respectively. The photonic initial-state corrections are identified as the part of the  $\mathcal{O}(\alpha)$  corrections that are proportional to the product of quark charges and comprise all contributions where the photon couples only to the quark or antiquark. Note that the QCD $\times$ photonic corrections even form a gauge-invariant part of the full off-shell calculation without PA.

- The factorizable final–final (FF)  $\mathcal{O}(\alpha_s\alpha)$  corrections include only counterterm corrections to the lepton–Z vertices and, in particular, do not receive contributions from real gluon or photon radiation. In [65] the explicit calculation of these corrections confirmed the expectation that their impact on differential cross sections is phenomenologically negligible.
- Non-factorizable (NF) corrections are induced by soft-photon exchange or emission connecting final-state leptons and initial-state quarks, combined with QCD  $\mathcal{O}(\alpha_s)$  corrections to Z-boson production. The non-trivial momentum flow of the soft photon between production and decay subprocesses, which implies that the squared matrix elements are not proportional to a squared Z propagator, gave rise to the terminology “non-factorizable”. Owing to a systematic cancellation between real and virtual NF corrections the numerical impact of these corrections on differential cross sections is at the sub-permille level [64] and therefore of no relevance for phenomenology.

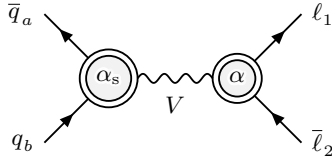
The four types of  $\mathcal{O}(\alpha_s\alpha)$  corrections in PA can be further classified into the usual NNLO contributions of types double-real, real–virtual, and double-virtual. Figure 1 shows the separation of the double-virtual corrections into IF, II, FF, and NF contributions; the corresponding separation of the double-real and real–virtual corrections is obvious.

## 2.2 Calculation of the factorizable initial–initial corrections

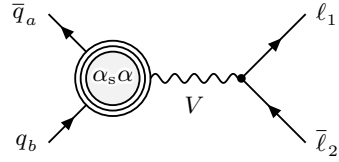
In this section we present the details of our calculation of the corrections of type II. The calculation of the corrections of types IF+FF and type NF can be found in Refs. [65] and [64], respectively. Since the PA for the factorizable corrections is based on amplitudes for the production and decay subprocesses, the implementation of the PA involves a projection of momenta to on-shell (OS) Z bosons in the subamplitudes (but not in the intermediate Z propagator), in order to maintain gauge invariance in the subamplitudes. The details of the OS mappings are discussed when they become relevant below.

The QCD  $\times$  photonic  $\mathcal{O}(\alpha_s\alpha_p)$  corrections of type II are proportional to the charge factors  $Q_q^2$  of the (anti)quarks and therefore gauge invariant even without applying the PA. In order to stay closer to the full calculation, we evaluate the QCD  $\times$  photonic corrections without employing the PA. However, for the QCD  $\times$  weak  $\mathcal{O}(\alpha_s\alpha_w)$  corrections we have to use the PA to preserve gauge invariance. Both for the QCD  $\times$  weak and the QCD  $\times$  photonic II corrections we have performed two independent calculations which produce results that are in mutual numerical agreement.

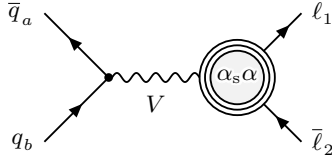
The double-real, real–virtual, and double-virtual contributions arising in the calculation of corrections of type II are depicted in Fig. 2. Initial–initial  $\mathcal{O}(\alpha_s\alpha_p)$  corrections



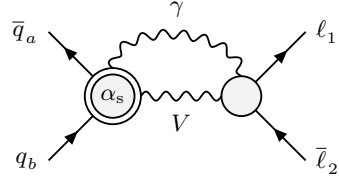
(a) Factorizable initial-final (IF) corrections



(b) Factorizable initial-initial (II) corrections



(c) Factorizable final-final (FF) corrections



(d) Non-factorizable (NF) corrections

Figure 1: The four types of corrections that contribute to the mixed QCD  $\times$  EW corrections in PA illustrated in terms of generic two-loop amplitudes. Simple circles symbolize tree structures, double circles one-loop corrections, and triple circles two-loop contributions.

demand a proper NNLO subtraction scheme as they involve two potentially unresolved particles in the final state. To this end, we employ antenna subtraction. The construction of antenna subtraction functions at  $\mathcal{O}(\alpha_s \alpha_p)$  is based on the subleading colour parts of the known  $\mathcal{O}(\alpha_s^2)$  antenna functions for the initial-final [86] and initial-initial [87, 88] cases. In contrast to the QCD  $\times$  photonic II corrections, in the QCD  $\times$  weak II corrections only one potentially unresolved particle is involved, and therefore the IR pole structure is of one-loop complexity, so that one-loop subtraction schemes are sufficient to handle the IR poles. In this case we have applied both antenna [82] and dipole subtraction [83] and compared the obtained results, which are in agreement.

### 2.2.1 Double-virtual corrections

The double-virtual corrections affect the underlying  $2 \rightarrow 2$  process

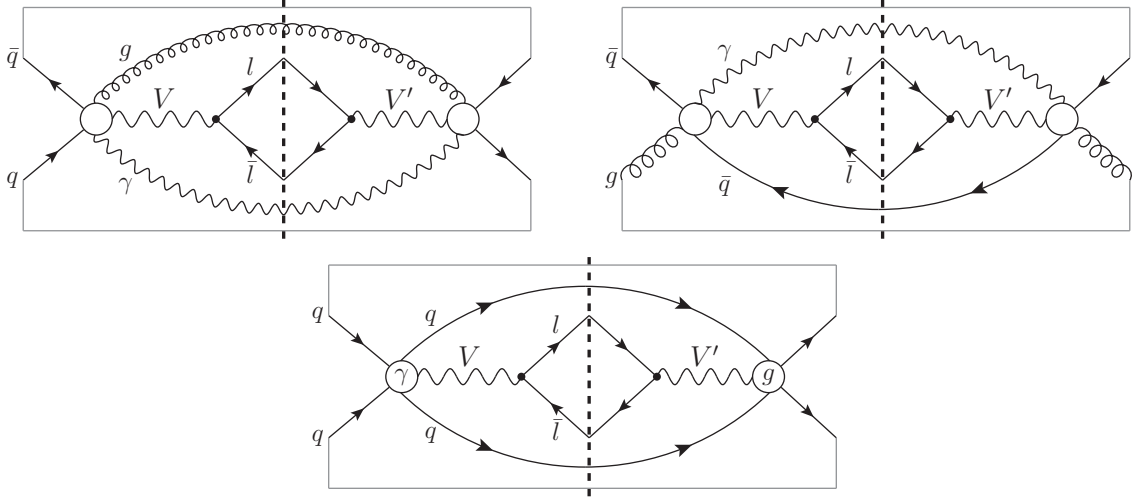
$$q(p_q, \sigma_q) + \bar{q}(p_{\bar{q}}, \sigma_{\bar{q}}) \rightarrow \ell^-(k_\ell, \tau_\ell) + \ell^+(k_{\bar{\ell}}, \tau_{\bar{\ell}}), \quad (2.1)$$

where the momenta and helicity labels of the respective particles are given in parentheses. The total incoming momentum is denoted  $q = p_q + p_{\bar{q}}$  in the following. All external fermions are taken massless, i.e.  $p_q^2 = p_{\bar{q}}^2 = k_\ell^2 = k_{\bar{\ell}}^2 = 0$ . In the following we will make use of the Mandelstam variables

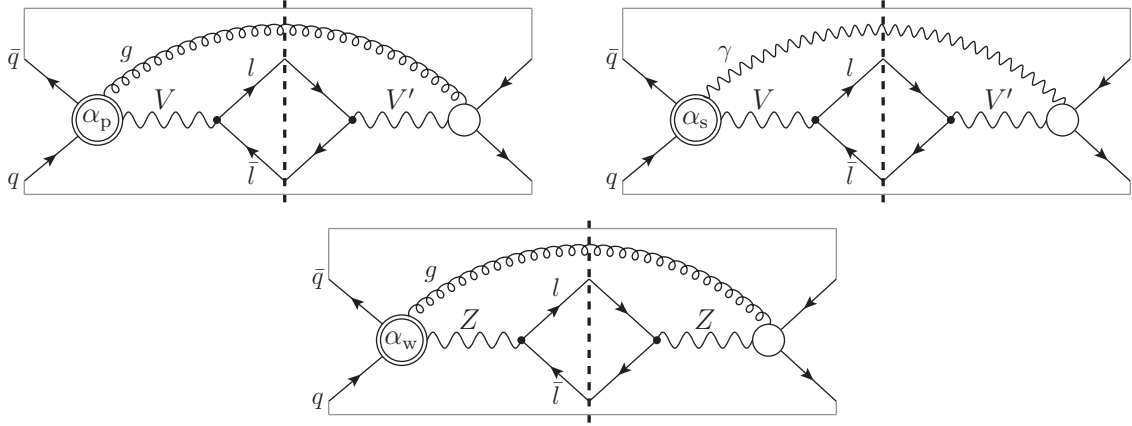
$$\hat{s} = (p_q + p_{\bar{q}})^2 = q^2, \quad \hat{t} = (p_q - k_\ell)^2, \quad \hat{u} = (p_q - k_{\bar{\ell}})^2. \quad (2.2)$$

The double-virtual II corrections to the  $q\bar{q} \rightarrow \ell\bar{\ell}$  matrix element receive contributions from QCD  $\times$  weak  $\mathcal{O}(\alpha_s \alpha_w)$  and QCD  $\times$  photonic  $\mathcal{O}(\alpha_s \alpha_p)$  corrections. The  $\mathcal{O}(\alpha_s \alpha_w)$  corrections to the  $Z\bar{q}q$  vertex are contained in the two-loop contribution to the renormalized  $Z\bar{q}q$  formfactors  $\hat{F}_\pm^{Z\bar{q}q}(q^2)$  for light quarks,

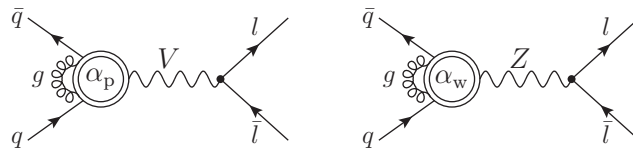
$$\Gamma_{R,\mu}^{Z\bar{q}q}(-q, p_{\bar{q}}, p_q) = e \sum_{\tau=\pm} \hat{F}_\tau^{Z\bar{q}q}(q^2) \gamma_\mu \omega_\tau, \quad \omega_\pm = \frac{1}{2}(1 \pm \gamma_5), \quad (2.3)$$



(a) Double-real  $\mathcal{O}(\alpha_s\alpha_p)$  II interference diagrams



(b) Real-virtual  $\mathcal{O}(\alpha_s\alpha_p)$  II (first line) and  $\mathcal{O}(\alpha_s\alpha_w)$  II (second line) interference diagrams



(c) Double-virtual  $\mathcal{O}(\alpha_s\alpha_p)$  and  $\mathcal{O}(\alpha_s\alpha_w)$  II diagrams

Figure 2: Various contributions to the gauge-invariant set of  $\mathcal{O}(\alpha_s\alpha_p)$  and  $\mathcal{O}(\alpha_s\alpha_w)$  II corrections, where  $V, V' = Z, \gamma$ . Double circles indicate one-loop corrections, simple circles indicate relevant tree structures, and simple circles with a “ $\gamma$ ” (“ $g$ ”) inside represent all possible connected tree-level diagrams of the process  $q_a q_a \rightarrow q_a q_a + V$  with an intermediate photon (gluon). An additional particle attached to a “one-loop blob”, as e.g. in Fig. 2c, means that the particle has to be inserted into the corresponding one-loop diagram in all possible ways.

where  $\Gamma_{R,\mu}^{Z\bar{q}q}$  is the renormalized  $Z\bar{q}q$  vertex function with off-shell  $Z$  momentum  $q$  projected onto massless external on-shell (anti)quarks  $q/\bar{q}$  and  $e$  is the elementary charge. For field-theoretical quantities and Standard Model fields and parameters we follow the notation and conventions of Ref. [66], if not defined otherwise. The LO contributions  $F_{LO,\tau}^{Z\bar{q}q}$  to the formfactors are given by

$$F_{LO,\tau}^{Z\bar{q}q} = g_q^\tau, \quad (2.4)$$

with the chiral couplings

$$g_f^+ = -\frac{Q_f s_w}{c_w}, \quad g_f^- = \frac{I_{w,f}^3 - Q_f s_w^2}{c_w s_w}, \quad (2.5)$$

where  $Q_f$  and  $I_{w,f}^3$  denote the electric charge and the third component of weak isospin of some fermion  $f$ , respectively. Here,  $s_w$  and  $c_w$  are the sine and cosine of the weak mixing angle, which is related to the masses  $M_W$  and  $M_Z$  of the W/Z bosons according to  $c_w = M_W/M_Z$ .

It is convenient to define the so-called reducible (red) parts of the  $\mathcal{O}(\alpha_s\alpha_w)$  contribution to the formfactors as the products of the renormalized one-loop QCD and weak contributions to the formfactors,

$$\hat{F}_{V_s \otimes V_w, \tau}^{Z\bar{q}q, \text{red}}(q^2) = \delta_{V_s}^{Z\bar{q}q}(q^2) \hat{F}_{V_w, \tau}^{Z\bar{q}q}(q^2), \quad (2.6)$$

where  $\delta_{V_s}^{Z\bar{q}q}(q^2)$  is the renormalized NLO QCD correction factor, e.g., given in Eq. (2.35) of Ref. [64], and the renormalized NLO weak formfactor contribution  $\hat{F}_{V_w, \tau}^{Z\bar{q}q}(q^2)$ . The latter decomposes into unrenormalized part  $F_{V_w, \tau}^{Z\bar{q}q}(q^2)$  and counterterm contribution  $\delta_{Z\bar{q}q, \text{weak}}^{\text{ct}, \tau}$ ,

$$\hat{F}_{V_w, \tau}^{Z\bar{q}q}(q^2) = F_{V_w, \tau}^{Z\bar{q}q}(q^2) + F_{LO, \tau}^{Z\bar{q}q} \delta_{Z\bar{q}q, \text{weak}}^{\text{ct}, \tau}. \quad (2.7)$$

Explicit expressions for the weak corrections and counterterms can, e.g., be found in Refs. [57].

To extract the genuine NNLO information contained in the full  $\mathcal{O}(\alpha_s\alpha_w)$  formfactor we define the irreducible (irred) contribution as the difference between the full  $\mathcal{O}(\alpha_s\alpha_w)$  and the reducible contributions to the formfactor,

$$\hat{F}_{V_s \otimes V_w, \tau}^{Z\bar{q}q, \text{irred}}(q^2) = \hat{F}_{V_s \otimes V_w, \tau}^{Z\bar{q}q}(q^2) - \hat{F}_{V_s \otimes V_w, \tau}^{Z\bar{q}q, \text{red}}(q^2), \quad (2.8)$$

where the corresponding diagrams are shown in Fig. 3. This irreducible contribution further decomposes into a ( $q^2$ -independent) counterterm part  $\hat{F}_{N_f \alpha_s \alpha_w, \tau}^{Z\bar{q}q, \text{irred}}$  containing all irreducible two-loop contributions with closed quark loops and an internal gluon and a part  $F_{V_s \otimes V_w, \tau}^{Z\bar{q}q, \text{irred}}(q^2)$  comprising all genuine two-loop corrections to the vertex and the external quark lines. For the  $N_f$ -enhanced counterterm part  $\hat{F}_{N_f \alpha_s \alpha_w, \tau}^{Z\bar{q}q, \text{irred}}$  we adopt the results of Ref. [76], where the  $\mathcal{O}(N_f \alpha_s \alpha)$  corrections to the full off-shell process have been calculated,

$$\hat{F}_{N_f \alpha_s \alpha_w, \tau}^{Z\bar{q}q, \text{irred}} = F_{LO, \tau}^{Z\bar{q}q} \delta_{Z\bar{q}q, (\alpha_s \alpha)}^{\text{ct}, \tau}, \quad (2.9)$$



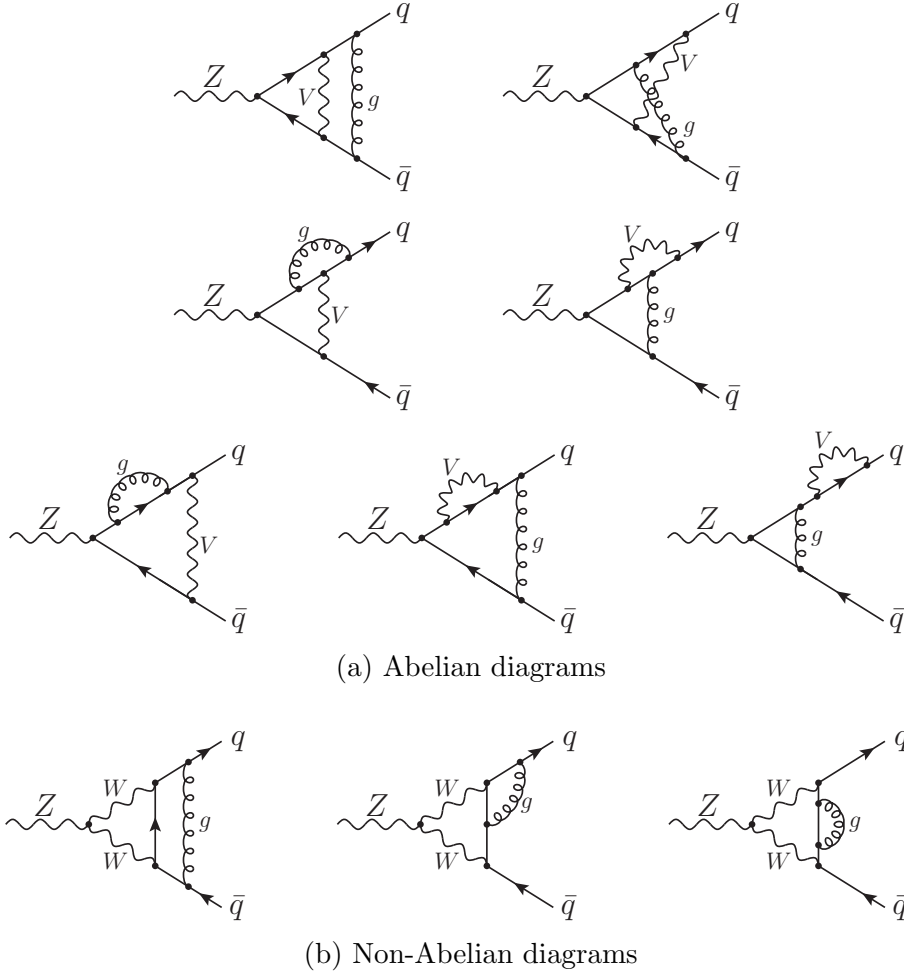


Figure 3: Example diagrams for the various  $\mathcal{O}(\alpha_s \alpha_w)$  two-loop contributions to the  $Z\bar{q}q$  vertex, where  $V = Z, W$ .

where the counterterm correction factor  $\delta_{Z\bar{f}f,(\alpha_s\alpha)}^{\text{ct},\tau}$  is given in Eq. (2.46) of Ref. [76].<sup>1</sup> The  $N_f$ -independent  $\mathcal{O}(\alpha_s \alpha_w)$  part  $F_{V_s \otimes V_w, \tau}^{Z\bar{q}q, \text{irred}}(q^2)$  is most conveniently formulated with two auxiliary functions, called  $\phi_A$  and  $\phi_{NA}$  in the following, which have been introduced and calculated in Ref. [81],

$$\begin{aligned}
F_{V_s \otimes V_w, +}^{Z\bar{q}q, \text{irred}}(q^2) &= C_F \frac{\alpha_s}{4\pi} \frac{\alpha}{4\pi} (g_q^+)^3 \phi_A(q^2/M_Z^2), \\
F_{V_s \otimes V_w, -}^{Z\bar{q}q, \text{irred}}(q^2) &= C_F \frac{\alpha_s}{4\pi} \frac{\alpha}{4\pi} \left( (g_q^-)^3 \phi_A(q^2/M_Z^2) + \frac{g_q^-}{2s_w^2} \phi_A(q^2/M_W^2) + I_{w,q}^3 \frac{c_w}{2s_w^3} \phi_{NA}(q^2/M_W^2) \right),
\end{aligned} \tag{2.10}$$

where  $C_F = 4/3$ .

We have performed a completely independent recalculation of the formfactors  $\phi_A$  and  $\phi_{NA}$ . The graphs for the two-loop vertex corrections were generated with FEYNARTS1.0 [89]. To express the amplitudes in terms of scalar two-loop master integrals

<sup>1</sup>Actually, the result given there is formulated in the complex-mass scheme. The translation to the real OS renormalization scheme used in this paper is, however, obvious.

the amplitudes were further algebraically reduced with inhouse MATHEMATICA routines combined with an integral reduction based on KIRA [90, 91]. The scalar master integrals were calculated via differential equations [92, 93] producing results in terms of Goncharov Polylogarithms (GPLs) [94, 95]. The GPLs are evaluated with an inhouse library that was checked against results from the programs CHAPLIN [96] and HANDYG [97]. Further details of our formfactor calculation as well as benchmark numbers are given in App. A. Our second, independent calculation of the  $\mathcal{O}(\alpha_s\alpha_w)$  corrections makes use of the results for the unrenormalized irreducible contribution to the formfactor as given in Ref. [81]. Appendix A also reports on a comparison between our formfactor results and the ones taken from Ref. [81], revealing numerical agreement if we numerically evaluate the analytical results of Ref. [81], although we cannot fully reproduce all benchmark numbers given there.

In summary, the  $\mathcal{O}(\alpha_s\alpha_w)$  contributions to the  $Z\bar{q}q$  formfactor defined in (2.3) decompose as

$$\begin{aligned}\hat{F}_{\alpha_s\alpha_w,\tau}^{Z\bar{q}q}(q^2) &= \hat{F}_{V_s\otimes V_w,\tau}^{Z\bar{q}q,\text{red}}(q^2) + \hat{F}_{V_s\otimes V_w,\tau}^{Z\bar{q}q,\text{irred}}(q^2) \\ &= \delta_{V_s}^{Z\bar{q}q}(q^2) \left[ F_{V_w,\tau}^{Z\bar{q}q}(q^2) + F_{\text{LO},\tau}^{Z\bar{q}q} \delta_{Z\bar{q}q,\text{weak}}^{\text{ct},\tau} \right] + F_{\text{LO},\tau}^{Z\bar{q}q} \delta_{Zff,(\alpha_s\alpha)}^{\text{ct},\tau} + F_{V_s\otimes V_w,\tau}^{Z\bar{q}q,\text{irred}}(q^2).\end{aligned}\quad (2.11)$$

In all contributions from closed quark loops, the full dependence on the bottom- and top-quark masses is kept. All other appearances of bottom quarks are connected to external quarks, which are all taken massless. In the one-loop formfactor  $F_{V_w,\tau}^{Z\bar{q}q}(q^2)$  and in the irreducible two-loop contribution  $F_{V_s\otimes V_w,\tau}^{Z\bar{q}q,\text{irred}}(q^2)$ , W-boson exchange leads to the appearance of top-quarks in the  $b\bar{b}$  channel, which is suppressed wrt. the other  $q\bar{q}$  channels. In  $F_{V_w,\tau}^{Z\bar{q}q}(q^2)$  the corresponding dependence on the top-quark mass  $m_t$  is kept, while  $m_t$  is set to zero in  $F_{V_s\otimes V_w,\tau}^{Z\bar{q}q,\text{irred}}(q^2)$ . To assess the validity of this approximation, we have also set  $m_t$  to zero in  $F_{V_w,\tau}^{Z\bar{q}q}(q^2)$  as well, which changes the QCD  $\times$  weak corrections to the  $M_{\ell\ell}$  distribution by less than 0.05% and to the forward-backward asymmetry  $A_{\text{FB}}(M_{\ell\ell})$  by about  $10^{-5}$  at most, which is both phenomenologically completely negligible.

The  $\mathcal{O}(\alpha_s\alpha_w)$  correction of type II to the squared  $q\bar{q} \rightarrow \ell\bar{\ell}$  amplitude,  $M_{V_s\otimes V_w,\text{II,PA}}^{q\bar{q}\rightarrow\ell\bar{\ell}}$ , is obtained from the interference between the genuine two-loop  $\mathcal{O}(\alpha_s\alpha_w)$  matrix element  $\mathcal{M}_{V_s\otimes V_w,\text{II,PA}}^{q\bar{q}\rightarrow\ell\bar{\ell}}$  and the LO matrix element  $\mathcal{M}_{\text{LO},Z}^{q\bar{q}\rightarrow\ell\bar{\ell}}$  and the interference of two one-loop matrix elements  $\mathcal{M}_{V_s,\text{I,PA}}^{q\bar{q}\rightarrow\ell\bar{\ell}}$  and  $\mathcal{M}_{V_w,\text{I,PA}}^{q\bar{q}\rightarrow\ell\bar{\ell}}$ , the former with an  $\mathcal{O}(\alpha_s)$  and the latter with an  $\mathcal{O}(\alpha_w)$  initial-state correction,

$$M_{V_s\otimes V_w,\text{II,PA}}^{q\bar{q}\rightarrow\ell\bar{\ell}} = 2 \text{Re} \left\{ \mathcal{M}_{V_s\otimes V_w,\text{II,PA}}^{q\bar{q}\rightarrow\ell\bar{\ell}} \left( \mathcal{M}_{\text{LO},Z}^{q\bar{q}\rightarrow\ell\bar{\ell}} \right)^* + \mathcal{M}_{V_s,\text{I,PA}}^{q\bar{q}\rightarrow\ell\bar{\ell}} \left( \mathcal{M}_{V_w,\text{I,PA}}^{q\bar{q}\rightarrow\ell\bar{\ell}} \right)^* \right\}. \quad (2.12)$$

In PA, the individual matrix elements in the last equation are obtained by employing the respective on-shell form factors  $F_{\dots}^{Z\bar{q}q}(q^2 = M_Z^2)$ ,

$$\mathcal{M}_{\text{LO},Z}^{q\bar{q}\rightarrow\ell\bar{\ell}} = e^2 \frac{F_{\text{LO},\sigma}^{Z\bar{q}q} g_{\ell}^{\sigma\tau}}{\hat{s} - \mu_Z^2} \mathcal{A}^{\sigma\tau}, \quad (2.13)$$

$$\mathcal{M}_{V_w,\text{I,PA}}^{q\bar{q}\rightarrow\ell\bar{\ell}} = e^2 \frac{\hat{F}_{V_w,\sigma}^{Z\bar{q}q}(M_Z^2) g_{\ell}^{\sigma\tau}}{\hat{s} - \mu_Z^2} \mathcal{A}^{\sigma\tau}, \quad \mathcal{M}_{V_s,\text{I,PA}}^{q\bar{q}\rightarrow\ell\bar{\ell}} = \delta_{V_s}^{Z\bar{q}q}(M_Z^2) \mathcal{M}_{\text{LO},Z}^{q\bar{q}\rightarrow\ell\bar{\ell}}, \quad (2.14)$$

$$\mathcal{M}_{V_s \otimes V_w, \text{II, PA}}^{q\bar{q} \rightarrow \ell\bar{\ell}} = e^2 \frac{\hat{F}_{\alpha_s \alpha_w, \sigma}^{Z\bar{q}q}(M_Z^2) g_\ell^\tau}{\hat{s} - \mu_Z^2} \mathcal{A}^{\sigma\tau}, \quad (2.15)$$

ensuring gauge invariance of the respective corrections. In the last equation  $\mu_Z^2 = M_Z^2 - iM_Z\Gamma_Z$  is the gauge-independent location of the Z-propagator pole, and  $\mathcal{A}^{\sigma\tau}$  are Dirac chains containing the information on the chiralities of the quark and lepton spinor chains  $\sigma$  and  $\tau$ , respectively; in Ref. [57] the  $\mathcal{A}^{\sigma\tau}$  were calculated to

$$\mathcal{A}^{\pm\pm} = 2\hat{u}, \quad \mathcal{A}^{\pm\mp} = 2\hat{t}. \quad (2.16)$$

Recall that  $\sigma$  and  $\tau$  fix the helicities of the external fermions ( $\sigma = \sigma_q = -\sigma_{\bar{q}}, \tau = \tau_\ell = -\tau_{\bar{\ell}}$ ), which are taken massless, so that the matrix-element contributions for different combinations  $\sigma\tau$  do not interfere.

Equation (2.12) contains products of weak and QCD one-loop corrections, raising the question whether the one-loop corrections are needed to higher orders in  $\epsilon = (4 - D)/2$  in dimensional regularization. This is, however, not the case, i.e. it is sufficient to evaluate all one-loop corrections to  $\mathcal{O}(\epsilon^0)$ . Since the weak one-loop corrections are finite, no  $\mathcal{O}(\epsilon)$  terms of the QCD one-loop corrections can produce relevant terms. On the other hand, the weak one-loop corrections eventually multiply the finite sum of QCD one-loop corrections and the integrated contributions of the QCD subtraction function (from antenna or dipole subtraction), so that  $\mathcal{O}(\epsilon)$  terms of the weak one-loop corrections cannot produce relevant terms either.

The contribution of double-virtual QCD  $\times$  photonic corrections to the squared  $q\bar{q} \rightarrow \ell\bar{\ell}$  amplitude is given by the interference of the genuine two-loop  $\mathcal{O}(\alpha_s\alpha_p)$  II amplitude and the LO amplitude, and by the interference between two one-loop amplitudes with initial-state corrections,

$$M_{V_s \otimes V_p, \text{II}}^{q\bar{q} \rightarrow \ell\bar{\ell}} = 2 \text{Re} \left\{ \mathcal{M}_{V_s \otimes V_p, \text{II}}^{q\bar{q} \rightarrow \ell\bar{\ell}} \left( \mathcal{M}_{\text{LO}, Z/\gamma}^{q\bar{q} \rightarrow \ell\bar{\ell}} \right)^* + \mathcal{M}_{V_s, \text{I}}^{q\bar{q} \rightarrow \ell\bar{\ell}} \left( \mathcal{M}_{V_p, \text{I}}^{q\bar{q} \rightarrow \ell\bar{\ell}} \right)^* \right\}. \quad (2.17)$$

Owing to parity invariance of QCD and QED, the QCD, the photonic, and the QCD  $\times$  photonic correction factors to the right- and left-handed formfactors of the  $Z\bar{q}q$  vertex coincide, so that the corrected matrix elements are proportional to the LO amplitude,

$$2 \text{Re} \left\{ \mathcal{M}_{V_s \otimes V_p, \text{II}}^{q\bar{q} \rightarrow \ell\bar{\ell}} \left( \mathcal{M}_{\text{LO}, Z/\gamma}^{q\bar{q} \rightarrow \ell\bar{\ell}} \right)^* \right\} = \delta_{V_s \otimes V_p}^{Z\bar{q}q, [2 \times 0]}(\hat{s}) \left| \mathcal{M}_{\text{LO}, Z/\gamma}^{q\bar{q} \rightarrow \ell\bar{\ell}} \right|^2, \quad (2.18)$$

$$2 \text{Re} \left\{ \mathcal{M}_{V_s, \text{I}}^{q\bar{q} \rightarrow \ell\bar{\ell}} \left( \mathcal{M}_{V_p, \text{I}}^{q\bar{q} \rightarrow \ell\bar{\ell}} \right)^* \right\} = \delta_{V_s \otimes V_p}^{Z\bar{q}q, [1 \times 1]}(\hat{s}) \left| \mathcal{M}_{\text{LO}, Z/\gamma}^{q\bar{q} \rightarrow \ell\bar{\ell}} \right|^2. \quad (2.19)$$

We recall that we evaluate these corrections without applying the PA, so that all amplitudes involve both Z-boson and photon exchange. The explicit expressions for the factorized correction factors can be extracted from the subleading colour contribution of the  $\mathcal{O}(\alpha_s^2)$  correction to the  $q\bar{q} \rightarrow \ell\bar{\ell}$  amplitude [98] or from the quark formfactor [99] using an abelianization procedure. We have recalculated the correction factors explicitly along the same lines as sketched in App. A for the QCD  $\times$  weak corrections.<sup>2</sup> The results are

$$\delta_{V_s \otimes V_p}^{Z\bar{q}q, [2 \times 0]}(\hat{s}) = 2Q_q^2 C_F \frac{\alpha_s \alpha}{\pi^2} C_\epsilon^2 \left( \frac{\mu^2}{\hat{s}} \right)^{2\epsilon} \left[ \frac{1}{4\epsilon^4} + \frac{3}{4\epsilon^3} + \frac{1}{\epsilon^2} \left( \frac{41}{16} - \frac{13\pi^2}{24} \right) \right] \quad (2.20)$$

<sup>2</sup>The coefficient of the  $\epsilon^{-1}$  contribution to  $\delta_{V_s \otimes V_p}^{Z\bar{q}q, [1 \times 1]}$  in [98] differs from our result by a sign in the term proportional to  $\zeta_3$ .

$$\begin{aligned}
& + \frac{1}{\epsilon} \left( \frac{221}{32} - \frac{3\pi^2}{2} - \frac{8}{3}\zeta_3 \right) + \left( \frac{1151}{64} - \frac{475\pi^2}{96} - \frac{29}{4}\zeta_3 + \frac{59\pi^4}{288} \right) + \mathcal{O}(\epsilon) \Big], \\
\delta_{V_s \otimes V_p}^{Z\bar{q}q, [1 \times 1]}(\hat{s}) &= 2Q_q^2 C_F \frac{\alpha_s \alpha}{\pi^2} \mathcal{C}_\epsilon^2 \left( \frac{\mu^2}{\hat{s}} \right)^{2\epsilon} \left[ \frac{1}{4\epsilon^4} + \frac{3}{4\epsilon^3} + \frac{1}{\epsilon^2} \left( \frac{41}{16} - \frac{\pi^2}{24} \right) \right. \\
& \left. + \frac{1}{\epsilon} \left( 7 - \frac{\pi^2}{8} - \frac{7}{6}\zeta_3 \right) + \left( 18 - \frac{41\pi^2}{96} - \frac{7}{2}\zeta_3 - \frac{7\pi^4}{480} \right) + \mathcal{O}(\epsilon) \right], \quad (2.21)
\end{aligned}$$

where  $\mathcal{C}_\epsilon = (4\pi)^\epsilon e^{-\epsilon\gamma_E}$ .

## 2.2.2 Real–virtual corrections

The factorizable real–virtual II  $\mathcal{O}(\alpha_s \alpha)$  corrections receive contributions from virtual photonic corrections to  $Z/\gamma^*$  production with real QCD radiation, from real photon radiation to the virtual QCD corrections to  $Z/\gamma^*$  production, and lastly from virtual weak corrections to  $Z$  production with real QCD radiation, as summarized in Fig. 2b. The types of contributing partonic channels of  $Z + \text{jet}$  and  $Z + \gamma$  production are given by

$$\bar{q}_a(p_a) + q_b(p_b) \rightarrow Z(p_Z) + g(k_g), \quad (2.22)$$

$$\bar{q}_a(p_a) + q_b(p_b) \rightarrow Z(p_Z) + \gamma(k_\gamma), \quad (2.23)$$

$$g(p_g) + q_b(p_b) \rightarrow Z(p_Z) + q_a(k_a), \quad (2.24)$$

$$g(p_g) + \bar{q}_a(p_a) \rightarrow Z(p_Z) + \bar{q}_b(k_b). \quad (2.25)$$

Note we have not included channels with photons in the initial state, since their impact is already suppressed at NLO. As described above, all QCD  $\times$  photonic II corrections are consistently evaluated for the full off-shell process with  $Z$  and  $\gamma$  exchange, while the amplitudes with a virtual weak and a real QCD correction have to be evaluated in PA to preserve gauge invariance.

The  $2 \rightarrow 3$  one-loop matrix elements are evaluated in two independent ways. In the first calculation the results for the virtual one-loop EW corrections to  $Z + \text{jet}$  production have been taken from the earlier calculation [100], and the virtual one-loop QCD corrections to  $Z + \gamma$  have been obtained via an abelianization of the NNLO QCD calculation [101]. In the second calculation FEYNARTS [102] is used to generate the amplitudes which are reduced to standard integrals using FORMCALC [103]. The one-loop integrals are numerically evaluated with the library COLLIER [104].

We now turn to the construction of the PA for the QCD  $\times$  weak II corrections, in particular to the issue of an appropriate OS projection of momenta to guarantee gauge-invariant subamplitudes. Having constructed the amplitudes for the virtual weak and real QCD correction to  $Z$  production in the  $\bar{q}q$  channel, we first construct a preliminary version of the PA amplitude from the  $Zg$ -production and  $Z$ -decay subamplitudes,

$$\widetilde{\mathcal{M}}_{V_w \otimes R_s, Z, \text{prod} \times \text{prod}}^{\bar{q}_a q_b \rightarrow \ell \bar{\ell}, \text{PA}} = \sum_{\lambda_Z} \frac{\mathcal{M}_{V_w \otimes R_s, \text{PA}}^{\bar{q}_a q_b \rightarrow g Z}(\lambda_Z) \mathcal{M}_{0, \text{PA}}^{Z \rightarrow \ell \bar{\ell}}(\lambda_Z)}{p_Z^2 - \mu_Z^2}, \quad (2.26)$$

where the tilde indicates that we still have to fix the OS projection of the external momenta. Rescaling all external momenta according to

$$\begin{aligned} p_i &\rightarrow \hat{p}_i = p_i \frac{M_Z}{\sqrt{2k_\ell k_{\bar{\ell}}}}, & i = a, b, g, \\ k_j &\rightarrow \hat{k}_j = k_j \frac{M_Z}{\sqrt{2k_\ell k_{\bar{\ell}}}}, & j = a, b, \ell, \bar{\ell}, g, \end{aligned} \quad (2.27)$$

preserves on-shellness of all (light-like) momenta and momentum conservation, and forces the new Z momentum  $\hat{p}_Z = \hat{k}_\ell + \hat{k}_{\bar{\ell}}$  on-shell,

$$\hat{p}_Z^2 = 2 \hat{k}_\ell \hat{k}_{\bar{\ell}} = M_Z^2. \quad (2.28)$$

Simply applying Eq. (2.27) to the residue of the resonance in Eq. (2.26) is, however, not sufficient to define a consistent PA, since we also have to guarantee a proper subtraction of all soft and collinear divergences in the IR limits. Since the subtraction function is constructed from the underlying  $2 \rightarrow 2$  scattering amplitudes in PA, the OS projections used in the  $2 \rightarrow 2$  and  $2 \rightarrow 3$  contributions are not independent.

In the calculation of the double-virtual corrections described in the previous section we have defined the OS projection in such a way that only the dimensionless  $Z\bar{q}q$  formfactor is forced to be on-shell, but not the Dirac chains  $\mathcal{A}^{\sigma\tau}$  of the amplitudes (and of course not the Z propagator containing the resonance). This variant ensures the same energy-scaling behaviour of the PA and off-shell amplitudes in the far off-shell regions up to logarithmic deviations contained in the corrections. Breaking the scaling behaviour would be prone to artefacts when evaluating the PA on the full phase space. The OS projection of the  $2 \rightarrow 2$  amplitudes can be summarized as follows,

$$\mathcal{M}_{Z,\text{PA}}^{2\rightarrow 2}(p_a, p_b, k_\ell, k_{\bar{\ell}}) = \frac{[\mathcal{M}_Z^{2\rightarrow 2} \cdot (p_Z^2 - \mu_Z^2)]|_{p_i \rightarrow \hat{p}_i, k_j \rightarrow \hat{k}_j}}{p_Z^2 - \mu_Z^2} \cdot \frac{2 k_\ell k_{\bar{\ell}}}{M_Z^2}, \quad (2.29)$$

where the last factor on the r.h.s. is used to restore the original scaling behaviour of the  $\mathcal{A}^{\sigma\tau}$  after the application of (2.27).

By the same reasoning, we have to rescale  $\widetilde{\mathcal{M}}_{V_w \otimes R_s, Z, \text{prod} \times \text{prod}}^{\bar{q}_a q_b \rightarrow \ell \bar{\ell}, \text{PA}}$  of Eq. (2.26) by a factor  $2 k_\ell k_{\bar{\ell}} / M_Z^2$  to restore the scaling behaviour of the spinor chains. However, we have yet to apply another factor  $M_Z / \sqrt{2 k_\ell k_{\bar{\ell}}}$  to compensate for the fact that the  $2 \rightarrow 3$  amplitudes contain another factor of (energy)<sup>-1</sup> that was rescaled by applying Eq. (2.27). If we did not include this compensation factor, some mismatch would arise with the OS-projected subtraction function which employs squared  $2 \rightarrow 2$  amplitudes in PA times a splitting factor of dimension (energy)<sup>-2</sup> that is based on the off-shell kinematics. In summary, the OS projection of the  $2 \rightarrow 3$  amplitudes reads

$$\mathcal{M}_{V_w \otimes R_s, Z, \text{prod} \times \text{prod}}^{\bar{q}_a q_b \rightarrow \ell \bar{\ell}, \text{PA}} = \frac{[\widetilde{\mathcal{M}}_{V_w \otimes R_s, Z, \text{prod} \times \text{prod}}^{\bar{q}_a q_b \rightarrow \ell \bar{\ell}, \text{PA}} \cdot (p_Z^2 - \mu_Z^2)]|_{p_i \rightarrow \hat{p}_i, k_j \rightarrow \hat{k}_j}}{p_Z^2 - \mu_Z^2} \cdot \sqrt{\frac{2 k_\ell k_{\bar{\ell}}}{M_Z^2}}. \quad (2.30)$$

This OS projection of the  $2 \rightarrow 3$  amplitudes is also in line with the integrated subtraction function which receives the same scaling as the  $2 \rightarrow 2$  contributions after integration over the off-shell phase space.

Note that the choice we made for the OS projection is not unique and different choices would be possible. For instance, we could have opted to keep also the Dirac structures on-shell. Different versions for the OS projection lead to results that formally differ at the order of the intrinsic uncertainty of the PA. However, it is important to construct the on-shell projection in a self-consistent way in order to guarantee a proper subtraction of all soft and collinear singularities between  $2 \rightarrow 3$  contributions and subtraction functions in the IR limits. The OS projection for  $2 \rightarrow 3$  processes, thus, implicitly fixes OS projection of all  $2 \rightarrow 2$  processes by this consistency requirement.

### 2.2.3 Double-real corrections

The double-real corrections are diagrammatically illustrated in Fig. 2a and are induced by diagrams with both an external gluon and photon or by diagrams with two additional external (anti)quarks and an internal photon, i.e. they are all part of the  $\text{QCD} \times \text{photonic}$   $\mathcal{O}(\alpha_s \alpha_p)$  II corrections, while  $\text{QCD} \times \text{weak}$  corrections do not contribute here.<sup>3</sup> Accordingly, we do not apply the PA in the calculation of double-real corrections. The types of channels that have to be considered are given by

$$\bar{q}_a(p_a) + q_b(p_b) \rightarrow Z(p_Z) + g(k_g) + \gamma(p_\gamma), \quad (2.31)$$

$$g(p_g) + q_b(p_b) \rightarrow Z(p_Z) + q_a(k_a) + \gamma(p_\gamma), \quad (2.32)$$

$$g(p_g) + \bar{q}_a(p_a) \rightarrow Z(p_Z) + \bar{q}_b(k_b) + \gamma(p_\gamma), \quad (2.33)$$

$$q_b(p_a) + q_b(p_b) \rightarrow Z(p_Z) + q_b(k_a) + q_b(k_b), \quad (2.34)$$

$$\bar{q}_a(p_a) + \bar{q}_a(p_b) \rightarrow Z(p_Z) + \bar{q}_a(k_a) + \bar{q}_a(k_b), \quad (2.35)$$

$$\bar{q}_a(p_a) + q_a(p_b) \rightarrow Z(p_Z) + \bar{q}_a(k_a) + q_a(k_b). \quad (2.36)$$

Again, we have not included channels with photons in the initial state, since their impact is already suppressed at NLO. The helicity amplitudes for the considered partonic channels were calculated using the spinor-helicity formalism, using the formulation of Ref. [105], and independently through the abelianization of the corresponding NNLO QCD amplitudes. Note that the double-real correction induced by the last diagram of Fig. 2a is only non-zero for the case where the quark chains close to a single loop, i.e. for the scattering of two identical quarks. Otherwise the interference amplitude vanishes owing to colour conservation.

---

<sup>3</sup>We note that the last diagram in Fig. 2a has a weak counterpart (with a Z boson instead of the photon in the blob) that is expected to be strongly suppressed and thus not considered further.

### 3 Numerical results

#### 3.1 Input parameters and event selection

The setup for the calculation is largely taken over from Refs. [64, 65]. The choice of input parameters closely follows Ref. [106],

$$\begin{aligned}
M_{W,\text{OS}} &= 80.385 \text{ GeV}, & \Gamma_{W,\text{OS}} &= 2.085 \text{ GeV}, \\
M_{Z,\text{OS}} &= 91.1876 \text{ GeV}, & \Gamma_{Z,\text{OS}} &= 2.4952 \text{ GeV}, \\
M_H &= 125.9 \text{ GeV}, & G_\mu &= 1.1663787 \times 10^{-5} \text{ GeV}^{-2}, \\
m_t &= 173.07 \text{ GeV}, & m_b &= 4.78 \text{ GeV}, \\
m_\mu &= 105.658369 \text{ MeV}.
\end{aligned}
\tag{3.1}$$

We convert the on-shell (OS) masses and decay widths of the vector bosons to the corresponding pole masses according to [66]

$$M_V = \frac{M_{V,\text{OS}}}{\sqrt{1 + \Gamma_{V,\text{OS}}^2/M_{V,\text{OS}}^2}}, \quad \Gamma_V = \frac{\Gamma_{V,\text{OS}}}{\sqrt{1 + \Gamma_{V,\text{OS}}^2/M_{V,\text{OS}}^2}}.
\tag{3.2}$$

The electromagnetic coupling constant is set according to the  $G_\mu$  scheme. The masses of the light quark flavours (u,d,c,s) and of the leptons are neglected throughout. The mass  $m_\mu$  of the muon is only needed in the evaluation of the logarithmically mass-singular FSR corrections for bare muons. The CKM matrix is chosen diagonal in the third generation, and the mixing between the first two generations of massless quarks cancels in cross sections by virtue of the unitarity of the CKM matrix. While b-quarks appearing in closed fermion loops have the mass  $m_b$  given in Eq. (3.1), external b-quarks are taken as massless.

We consider  $\mu^- \mu^+$  production in pp collisions at a centre-of mass energy of 13 TeV. For the PDFs we consistently use the NNPDF3.1 set [107], i.e. the NLO and NNLO QCD and QCD  $\times$  EW corrections are evaluated using the NNPDF31\_nlo\_as\_0118\_luxqed set, which also includes  $\mathcal{O}(\alpha)$  corrections. The value of the strong coupling  $\alpha_s(M_Z) = 0.118$  is dictated by the choice of this PDF set. The renormalization and factorization scales are set equal, with a fixed value given by the Z-boson mass,

$$\mu_R = \mu_F = M_Z.
\tag{3.3}$$

For the experimental identification of the DY process we impose the following cuts on the transverse momenta and rapidities of the charged leptons,

$$k_{T,\ell^\pm} > 25 \text{ GeV}, \quad |y_{\ell^\pm}| < 2.5.
\tag{3.4}$$

We further apply a cut on the invariant mass  $M_{\ell\ell}$  of the lepton pair,

$$M_{\ell\ell} > 50 \text{ GeV},
\tag{3.5}$$

in order to avoid the photon pole at  $M_{\ell\ell} \rightarrow 0$ .

In the following, we distinguish two alternative treatments of photon radiation off leptons: “bare muons” and “dressed leptons”. In the bare-muon case, no recombination of

leptons and nearly collinear photons is performed, reflecting the experimental situation which allows for the detection of isolated muons. In the dressed-lepton case, collinear photon–lepton configurations are treated inclusively using a photon-recombination procedure. As a result, the numerical predictions do not contain large logarithms of the lepton mass, which can be set to zero. The dressed-lepton results are appropriate mostly for electrons in the final state. In detail, for dressed leptons a photon recombination procedure analogous to the one used in Refs. [49, 57] is applied:

1. Photons close to the beam with a rapidity  $|\eta_\gamma| > 3$  are treated as beam remnants and are not further considered in the event selection.
2. For the photons that pass the first step, the angular distance to the charged leptons  $R_{\ell^\pm\gamma} = \sqrt{(\eta_{\ell^\pm} - \eta_\gamma)^2 + \Delta\phi_{\ell^\pm\gamma}^2}$  is computed, where  $\Delta\phi_{\ell^\pm\gamma}$  denotes the azimuthal angle difference of the lepton and photon in the transverse plane. If the distance  $R_{\ell^\pm\gamma}$  between the photon and the closest lepton is smaller than  $R_{\ell^\pm\gamma}^{\text{rec}} = 0.1$ , the photon is recombined with the lepton by adding the respective four-momenta,  $\ell^\pm(k_i) + \gamma(k) \rightarrow \ell^\pm(k_i + k)$ .
3. Finally, the event selection cuts from Eqs. (3.4)–(3.5) are applied to the resulting event kinematics.

### 3.2 Corrections to differential distributions

In this section we discuss our results on the corrections to muon pair production ( $\ell = \mu$ ) and to the production of a dressed lepton pair for the distributions in the invariant mass  $M_{\ell\ell}$  of the  $\bar{\ell}\ell$  pair, the transverse momentum  $k_{T,\ell}$  of one of the leptons, and the rapidity  $y_{\ell\ell}$  of the  $\bar{\ell}\ell$  pair. By default, relative corrections  $\delta$  are normalized to full off-shell LO distributions in the following. Whenever of relevance, we show both results for the event selection without or with photon recombination, denoted “bare muons” and “dressed leptons”, respectively, in the following.

We start out by showing the NLO QCD and NLO EW corrections in Fig. 4, recalculated in the setup described in the previous section. In the following, all LO, NLO, and NNLO cross sections are evaluated with the same PDF set, in order to make the impact of all types of corrections most transparent, without being affected by differences in the PDFs. The LO and NLO predictions are calculated using the complex-mass scheme [66, 108] for treating the Z-boson resonance, as described in Ref. [57] in detail, and the PA is not used in any of the NLO corrections. Owing to the suppression of the contribution from  $\gamma\gamma$  initial states, we only include the contributions of the  $q\bar{q}$  channels in the LO cross section and consider the LO  $\gamma\gamma$  contribution as part of the corrections. We denote as “ $\gamma$ -ind.” the sum of the LO ( $\gamma\gamma$ ) and NLO ( $q\gamma/\bar{q}\gamma$ ) photon-induced contributions. As will be illustrated in the following, the photon-induced contributions are strongly suppressed with no particular enhancement mechanism such that corrections beyond NLO, i.e. at  $\mathcal{O}(\alpha_s\alpha)$ , can be safely neglected for all phenomenological purposes.<sup>4</sup>

The decomposition of the NLO EW corrections into contributions from photonic final-state radiation (FSR), photonic initial–final interference effects (IF), photonic initial-state

---

<sup>4</sup>The omission of higher-order corrections to both the di-photon and other photon-induced contributions is further supported by Ref. [78], see e.g. Table I.



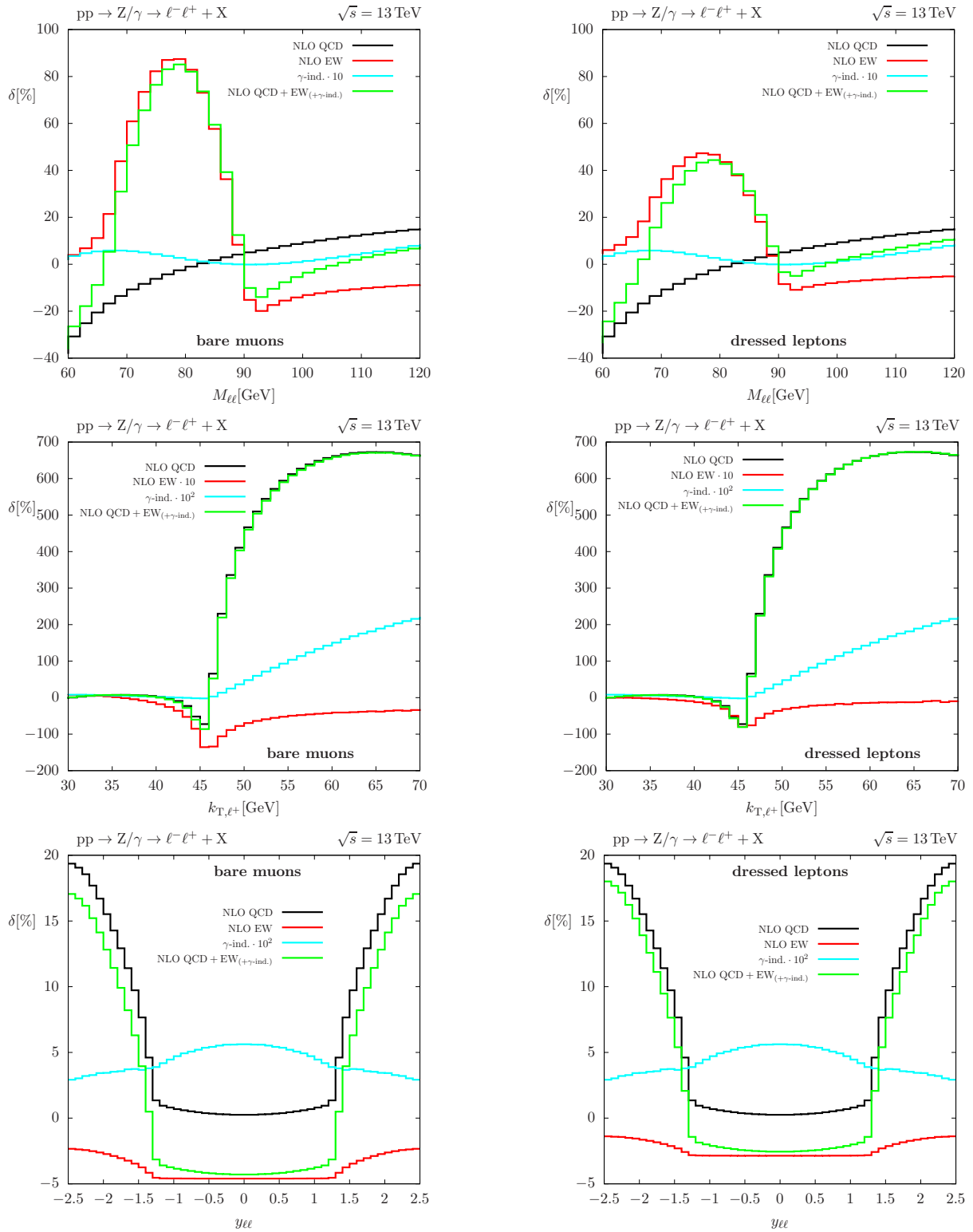


Figure 4: Relative NLO QCD (black), NLO EW (red),  $\gamma$ -induced (sum of LO  $\gamma\gamma$  and NLO  $q\gamma/\bar{q}\gamma$  contributions in cyan), and full NLO (green) corrections (normalized to LO) to various distributions for bare muons (l.h.s.) and for dressed leptons (r.h.s.).

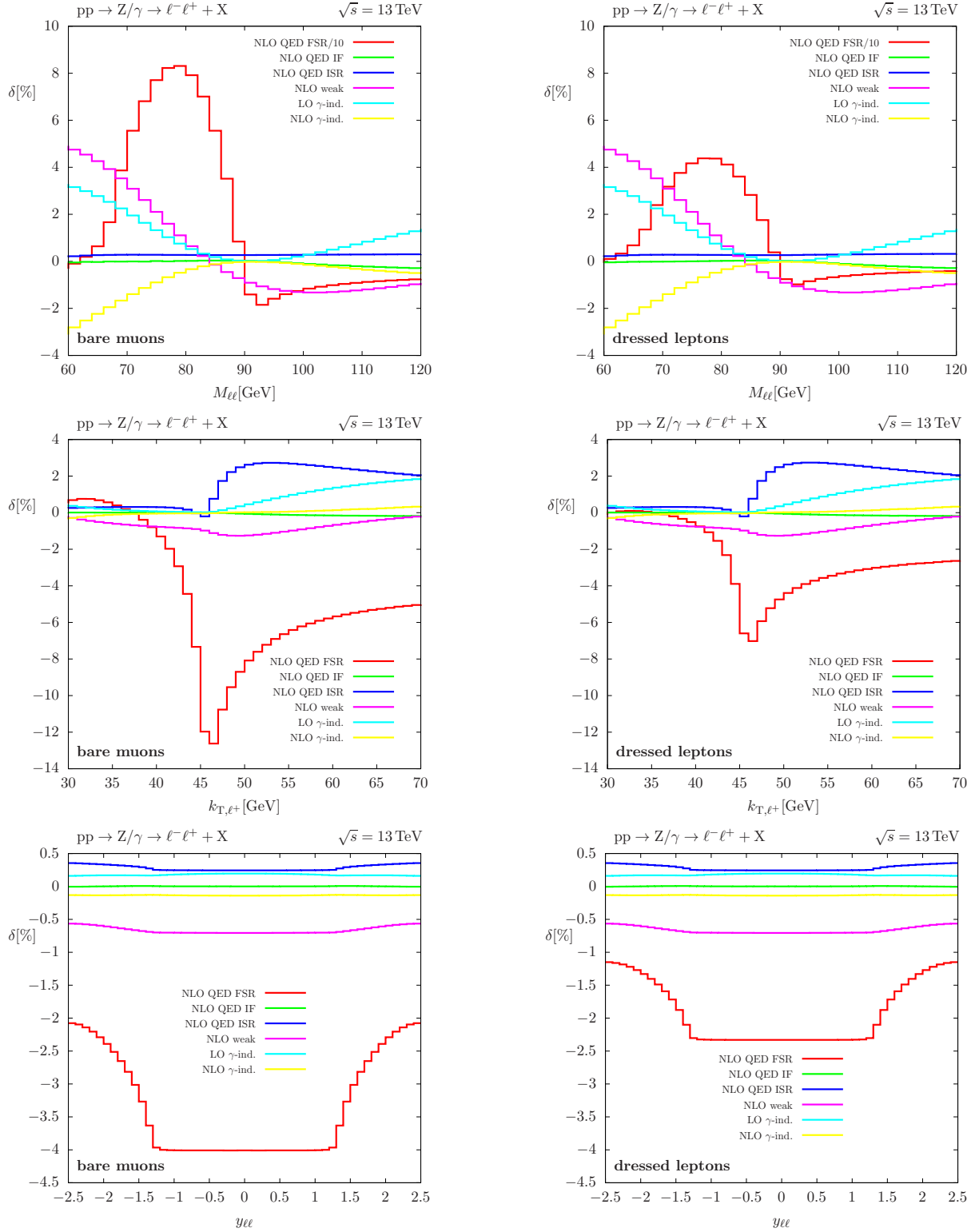


Figure 5: Decomposition of the NLO EW corrections (normalized to LO) into photonic FSR (red), photonic IF interference effects (green), photonic ISR (blue), and weak corrections (magenta), as well as relative corrections from LO  $\gamma\gamma$  (cyan) and NLO  $q\gamma/\bar{q}\gamma$  (yellow) initial states.

radiation (ISR), and purely weak corrections (weak) are shown in Fig. 5. The LO  $\gamma\gamma$  contribution as well as the NLO correction induced by  $q\gamma/\bar{q}\gamma$  initial states are illustrated in Fig. 5 separately as well. Of course, similar results have been shown in several places in the literature (see, e.g., Ref. [57]), but recalling these results facilitates the discussion of the  $\mathcal{O}(\alpha_s\alpha)$  corrections below.

The EW corrections to the  $M_{\ell\ell}$  distributions show the well-known radiative tail below the resonance at  $M_{\ell\ell} = M_Z$ , which is dramatically enhanced due to the collinear singularity  $\propto \alpha \ln(m_\ell/M_Z)$  in the FSR contribution if no photon recombination is applied. The fact that the radiative tail does not extend below  $M_{\ell\ell}$  values of about 68 GeV is an effect of the acceptance cuts on the lepton transverse momenta  $k_{T,\ell^\pm}$  of 25 GeV. The major part of all Z bosons is produced on shell, so that before FSR most leptons carry  $k_{T,\ell^\pm}$  of at most  $M_Z/2$ . At NLO, collinear FSR reduces one of the lepton momenta by a factor  $z$  ( $0 < z < 1$ ), so that  $M_{\ell\ell}^2$  is given by  $zM_Z^2$  after FSR. The maximal value of the reduced  $k_{T,\ell^\pm}$  is  $zM_Z/2$ , corresponding to a Z-boson decay transverse to the beams. Thus, for  $k_{T,\ell^\pm} = zM_Z/2 < 25$  GeV, which corresponds to  $M_{\ell\ell} = \sqrt{z}M_Z < 68$  GeV, events with an on-shell Z boson and collinear FSR off a lepton cannot pass the acceptance cut any more, which leads to a strong suppression of the FSR correction for such invariant masses  $M_{\ell\ell}$ . The photon recombination described in the previous section mitigates the FSR corrections by roughly a factor 2, i.e. the mass-singular logarithm is effectively replaced by  $\sim \ln R_{\ell^\pm\gamma}^{\text{rec}} = \ln(0.1)$ . The remaining photonic corrections (IF, ISR) are at the sub-percent level, the weak corrections at the few-percent level. The corrections induced by  $\gamma\gamma$  and  $q\gamma/\bar{q}\gamma$  initial states are largely suppressed on resonance (the  $\gamma\gamma$  channel does not develop a Z resonance at all), but typically matter at the percent level in a window of a width of 10–20 GeV around the Z-boson resonance.

The distribution in the transverse momentum of a lepton at LO is dominated by resonant Z production for  $k_{T,\ell} \lesssim M_Z/2$ , where all NLO corrections are moderate; the largest EW effects are again due to FSR. For larger  $k_{T,\ell} \gtrsim M_Z/2$  the QCD corrections develop “giant  $K$ -factors” [109], since the jet recoil in the real QCD corrections allows for the population of the region with  $k_{T,\ell} > M_Z/2$  by events with resonant Z bosons. The  $\gamma\gamma$ - and  $q\gamma/\bar{q}\gamma$ -induced corrections only amount to some  $\sim 0.1\%$  for transverse momenta below the Jacobian peak. For large transverse momenta, the same is true for the relative corrections normalized to the full (QCD-corrected) differential cross section.

Finally, the NLO corrections to the rapidity distribution of the Z boson resemble the moderate corrections to the integrated cross section in the central part of the distribution, i.e. for  $|y_{\ell\ell}| \lesssim 1.3$ . The corrections from  $\gamma\gamma$  and  $q\gamma/\bar{q}\gamma$  initial states only contribute at the level of 0.1–0.2% over the whole rapidity range.

Figure 6 shows two types of higher-order EW corrections beyond NLO: First, the FSR effects induced by collinear multi-photon emission off the leptons in the structure function approach [110–115]<sup>5</sup> based on leading logarithms up to  $\mathcal{O}(\alpha^3)$  with the NLO contribution subtracted. Second, the leading NNLO EW effects from the universal corrections induced by the running of the electromagnetic coupling ( $\Delta\alpha$ ) and by corrections to the  $\rho$ -parameter ( $\Delta\rho$ ). The precise definition of the two types of corrections can be found in Sects. 3.4.3 and 3.4.1 of Ref. [57], respectively. The corrections shown in Fig. 6 are obtained for bare muons. For dressed leptons the FSR effects based on leading-log struc-

<sup>5</sup>Note that Ref. [113] contains errors that have been addressed in Refs. [116, 117].

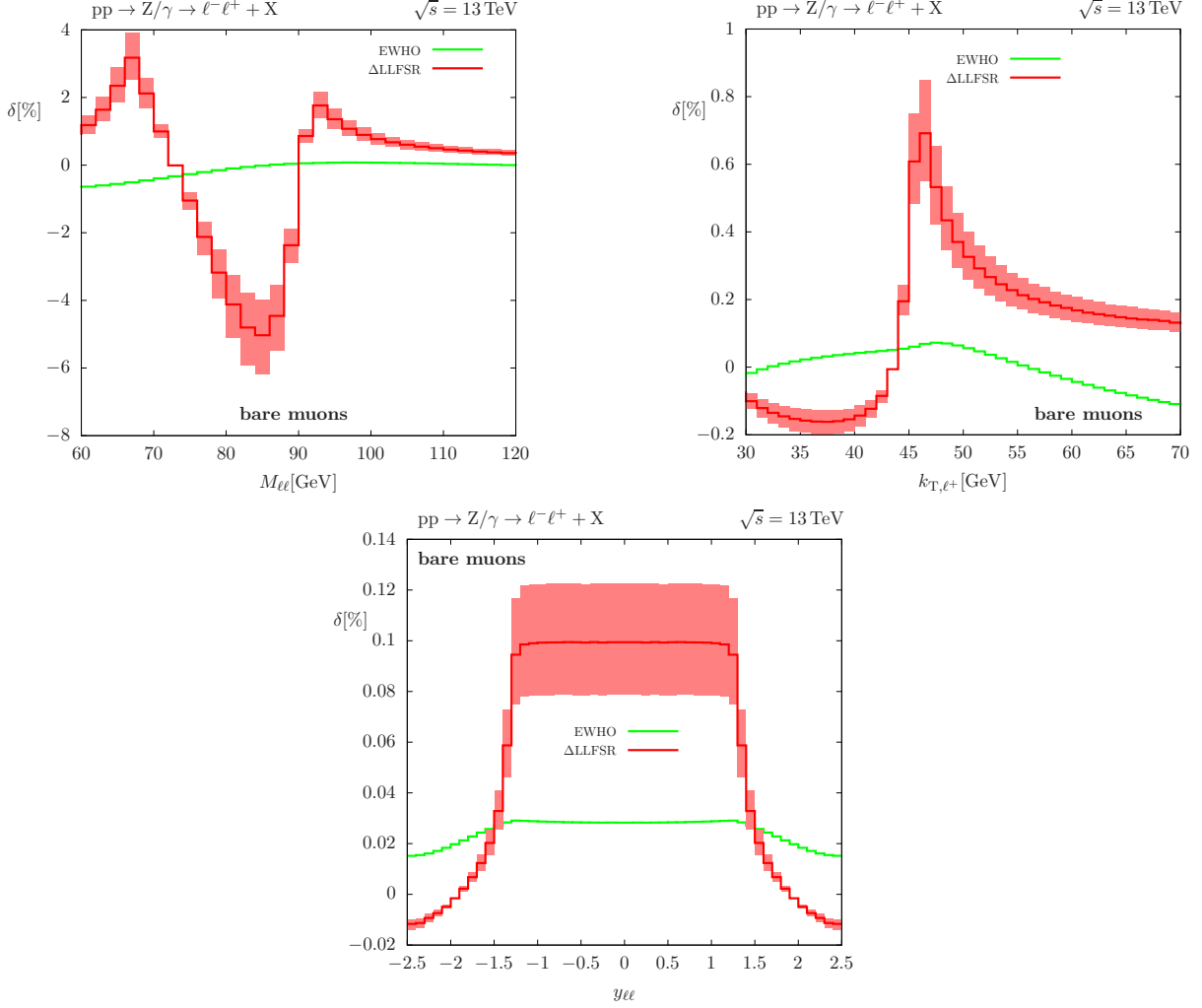


Figure 6: Relative higher-order photonic FSR effects ( $\Delta\text{LLFSR}$ , red), i.e. the NLO contribution is subtracted, and universal EW higher-order corrections (EWHO, green), both normalized to LO. The red band illustrates the scale uncertainty of the LLFSR correction by varying the central FSR scale  $\mu_{\text{FSR}} = M_Z$  up and down by a factor 2.

ture functions vanish, and the leading universal EW corrections would be identical to the ones for bare muons, because these corrections do not involve photon radiation. The most notable higher-order EW effect shown in Fig. 6 arises from multi-photon correction to the  $M_{\ell\ell}$  distribution, with an impact on the radiative tail at the level of 5%. Note also that the uncertainty arising from the scale  $\mu_{\text{FSR}}$  of the multi-photon effects that is not unambiguously fixed in leading logarithmic approximation is not completely negligible in the  $M_{\ell\ell}$  distribution.

Given that the dominant EW corrections arise from FSR corrections, we compare in Fig. 7 the NLO prediction to the one obtained using the PHOTOS [118] QED shower on top of the LO prediction. This allows to assess the performance of a tool commonly employed in the experimental measurements and the potential impact of multi-photon emissions that go beyond the structure-function approach discussed above. As anticipated, FSR

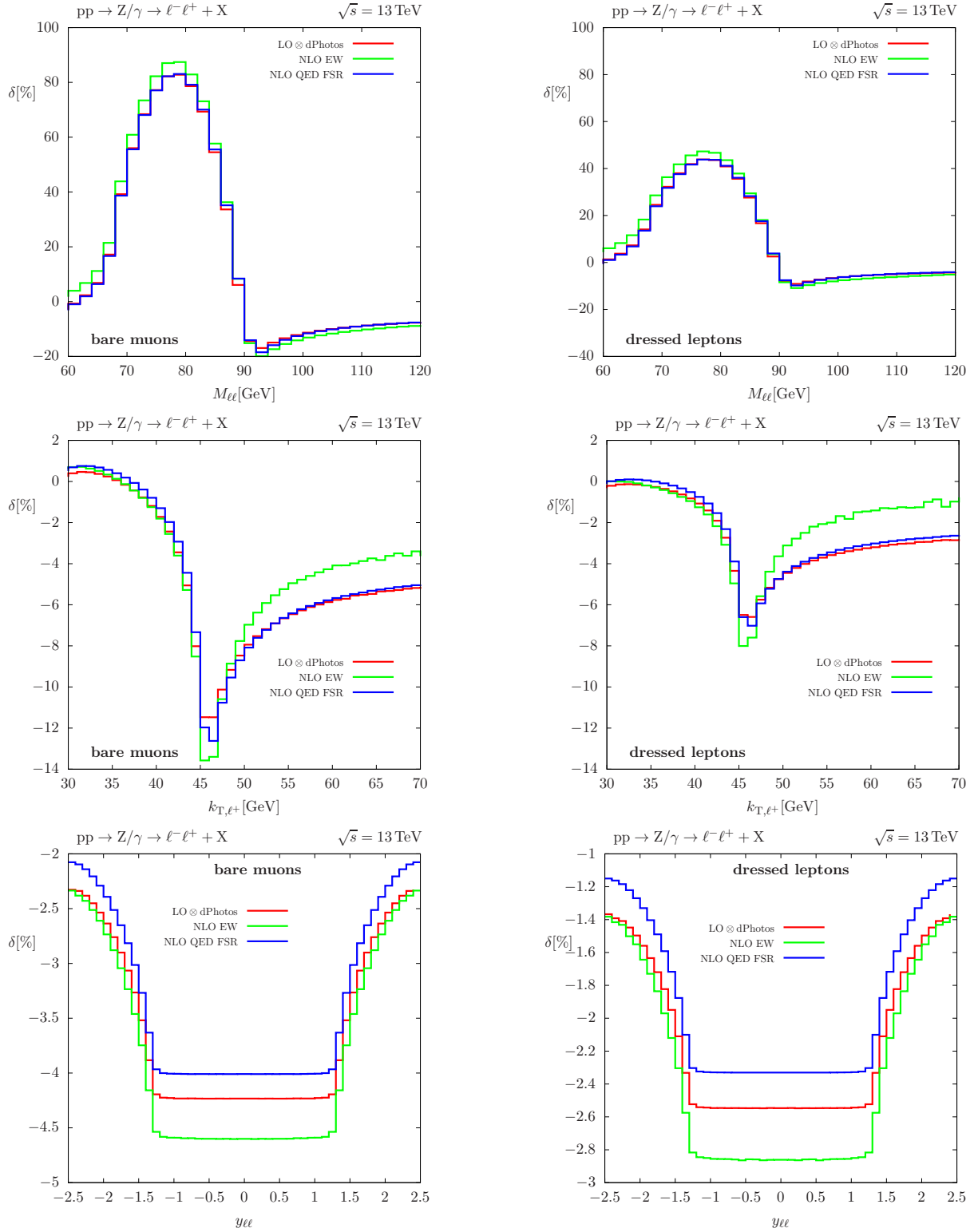


Figure 7: NLO EW (green) and  $\text{LO}_{\text{QCD}} \otimes \text{dPhotos}$  (red) corrections, normalized to LO.

effects are well captured by the PHOTOS tool, agreeing very well with the NLO QED FSR part of our calculation. NLO EW effects that go beyond FSR, i.e. ISR and initial-final QED effects and genuine weak corrections, on the other hand, are not included and thus not captured by the naive  $\text{LO} \otimes \text{PHOTOS}$  prediction. Small differences in the normalisation, as can be seen in the  $y_{\ell\ell}$  distribution can likely be attributed to multi-photon effects and the choice of  $\alpha$  scheme within the QED shower.

The NNLO QCD  $\times$  EW corrections in PA are shown in Fig. 8 together with their by far dominating contribution of type IF, which was already calculated in Ref. [65]. In the regions that are dominated by the Z resonance, the IF QCD  $\times$  EW corrections are typically one to a few percent and thus phenomenologically important and even larger than the NNLO QCD corrections, which we have been evaluated using the results of Ref. [101]. Note that the large radiative tail for  $M_{\ell\ell} \lesssim M_Z$ , where the QCD  $\times$  EW corrections grow to  $\sim 5\text{--}10\%$ , are still calculable in PA, because these effects are dominated by photonic FSR off the leptons that result from nearly resonant Z bosons. The shape of the QCD  $\times$  EW correction to the  $M_{\ell\ell}$  distribution is widely inherited from the product of the photonic FSR effect at  $M_{\ell\ell}$  and the QCD ISR correction at  $M_{\ell\ell} \approx M_Z$ . The only exception is the narrow peak slightly below  $M_{\ell\ell} \sim 68$  GeV, which is a fixed-order artefact from soft-gluon emission. To understand the origin of this peak, recall the explanation of the truncation of the FSR radiative tail observed in Fig. 4 below the Z resonance at  $M_{\ell\ell} \sim 68$  GeV. For smaller  $M_{\ell\ell}$  one of the decay leptons of a resonant Z boson cannot pass the cuts on  $k_{T,\ell^\pm}$  at NLO. At NNLO QCD  $\times$  EW, jet emission before the formation of the Z resonance leads to a recoil of the Z boson that is transferred to the decay leptons. Thus, near the edge at  $M_{\ell\ell} \sim 68$  GeV, relatively soft gluon emission can be enough to allow an event to pass the  $k_{T,\ell^\pm}$  cuts while corresponding events with virtual gluon exchange and LO kinematics in the Z production process still do not pass the cuts. This mismatch leads to the sharp peak for  $M_{\ell\ell}$  values slightly below the edge of the radiative QED FSR tail. Soft-gluon resummation or possibly an adjustment of fiducial cuts or of the event selection would largely mitigate this artefact, but this is beyond the scope of this paper.

As mentioned in the introduction, the setup of our calculation coincides with the one used in Ref. [78], where the  $\mathcal{O}(\alpha_s\alpha)$  corrections have been evaluated for bare muons without applying the PA. Overlaying our relative corrections to the  $M_{\ell\ell}$  distribution shown in the top-left plot of Fig. 8 with the corresponding plot in Fig. 2 of Ref. [78] reveals agreement within statistical fluctuation.<sup>6</sup> Note that this agreement also confirms our expectation that  $\mathcal{O}(\alpha_s\alpha)$  corrections induced by photons in the initial state, which are neglected in our calculation but included in the results of Ref. [78], are negligible.

In the  $k_{T,\ell}$  distribution the only significant effect of  $\sim 10\%$  appears at  $k_{T,\ell} \lesssim M_Z/2$  where the region of resonant Z bosons sets in. Note that for  $k_{T,\ell} > M_Z/2$  the plots overestimate the impact of the corrections because of their normalization to the LO distribution. Normalizing the corrections to the QCD-corrected differential cross section would reveal that the impact of QCD  $\times$  EW corrections is back to the few-percent level. As for the applicability of the PA for  $k_{T,\ell} > M_Z/2$ , where the LO distribution receives only contri-

---

<sup>6</sup>In the invariant-mass window  $70 \text{ GeV} < M_{\ell\ell} < 110 \text{ GeV}$  the good agreement holds, even though our PA takes into account only Z-boson exchange LO diagrams, i.e. we do not reweight the full LO cross section with Z-boson and photon exchange by some PA correction factor, as suggested in Eqs. (12,13) of Ref. [77].

butions from off-shell Z bosons, we still expect a good approximative quality of the PA, because the recoil from QCD ISR effects, which is part of the QCD  $\times$  EW corrections, allows for the population of this phase-space region by resonant Z bosons. Comparing our PA results on corrections to the  $k_{T,\ell}$  distribution shown in the left–middle plot of Fig. 8 to the corresponding results of Ref. [78] for bare muons, shown in their Fig. 1, we again find agreement within statistical fluctuations.

Finally, the QCD  $\times$  EW corrections to the  $y_{\ell\ell}$  distribution are about 0.5–1% and, thus, phenomenologically less important in the central region, where most of the events are concentrated.

The QCD  $\times$  EW corrections other than the IF contribution, i.e. the corrections of types II (calculated in this paper), NF [64], and FF [65] are depicted in Fig. 9. For the shown window around the Z resonance in the  $M_{\ell\ell}$  distribution and in the whole  $y_{\ell\ell}$  distribution, these contributions never exceed 0.2% and are phenomenologically not relevant in the absolute predictions of the differential cross sections. Only the II corrections to the  $k_{T,\ell}$  distribution gain some relevance, reaching the 1% level near  $k_{T,\ell} \sim M_Z/2$ . Recall again that for larger  $k_{T,\ell}$  the corrections should be normalized to the QCD-corrected prediction for an assessment of their true impact.

Figure 10 compares the IF factorizable corrections with an approximation obtained by folding the NLO QCD *correction*,  $\text{dNLO}_{\text{QCD}}$ , with the PHOTOS QED shower. In this way, terms of  $\mathcal{O}(\alpha_s\alpha)$  are generated that can be contrasted with the PA calculation. Overall, we observe a good qualitative agreement between the two predictions, further supporting our observation that the dominant effects at this order arise from FSR QED effects. Moreover, the good agreement hints that the impact of multi-photon emissions beyond what is captured in our calculation is likely not of high phenomenological relevance. As we will see in the next section, the agreement seen here in the absolute predictions degrades visibly in the case of the forward–backward asymmetry  $A_{\text{FB}}$ .

### 3.3 Corrections to the Forward–backward asymmetry

The forward–backward (FB) asymmetry for  $\ell^+\ell^-$  production at the LHC is defined as [46, 48]

$$A_{\text{FB}}(M_{\ell\ell}) = \frac{\sigma_{\text{F}}(M_{\ell\ell}) - \sigma_{\text{B}}(M_{\ell\ell})}{\sigma_{\text{F}}(M_{\ell\ell}) + \sigma_{\text{B}}(M_{\ell\ell})} \quad (3.6)$$

with

$$\sigma_{\text{F}}(M_{\ell\ell}) = \int_0^1 \text{d}\cos\theta^* \frac{\text{d}\sigma}{\text{d}\cos\theta^*}, \quad \sigma_{\text{B}}(M_{\ell\ell}) = \int_{-1}^0 \text{d}\cos\theta^* \frac{\text{d}\sigma}{\text{d}\cos\theta^*}. \quad (3.7)$$

The angle  $\theta^*$  is the so-called Collins–Soper (CS) angle, which is defined by [46, 119]

$$\cos\theta^* = \frac{|k_{\ell\ell}^3|}{k_{\ell\ell}^3} \frac{2}{M_{\ell\ell} \sqrt{M_{\ell\ell}^2 + k_{T,\ell\ell}^2}} \left( k_{\ell}^+ k_{\bar{\ell}}^- - k_{\bar{\ell}}^+ k_{\ell}^- \right), \quad (3.8)$$

where

$$k_{\ell\ell}^\mu = k_{\ell}^\mu + k_{\bar{\ell}}^\mu, \quad k_j^\pm = \frac{1}{\sqrt{2}}(k_j^0 \pm k_j^3), \quad j = \ell, \bar{\ell}, \quad (3.9)$$

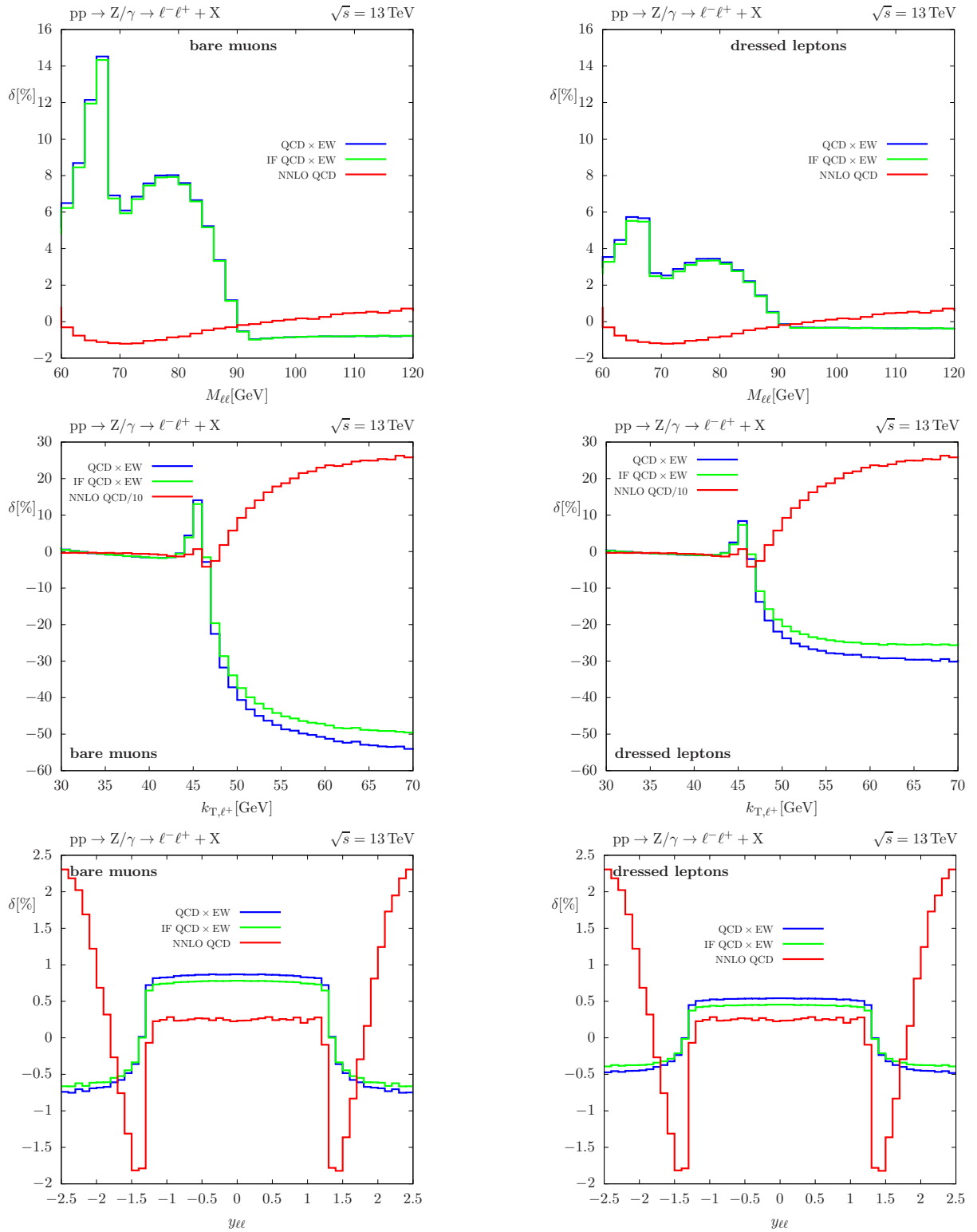


Figure 8: Relative NNLO QCD corrections (red) as well as a comparison of the full QCD  $\times$  EW corrections in PA (blue) with its IF contribution (green); all corrections are normalized to LO.



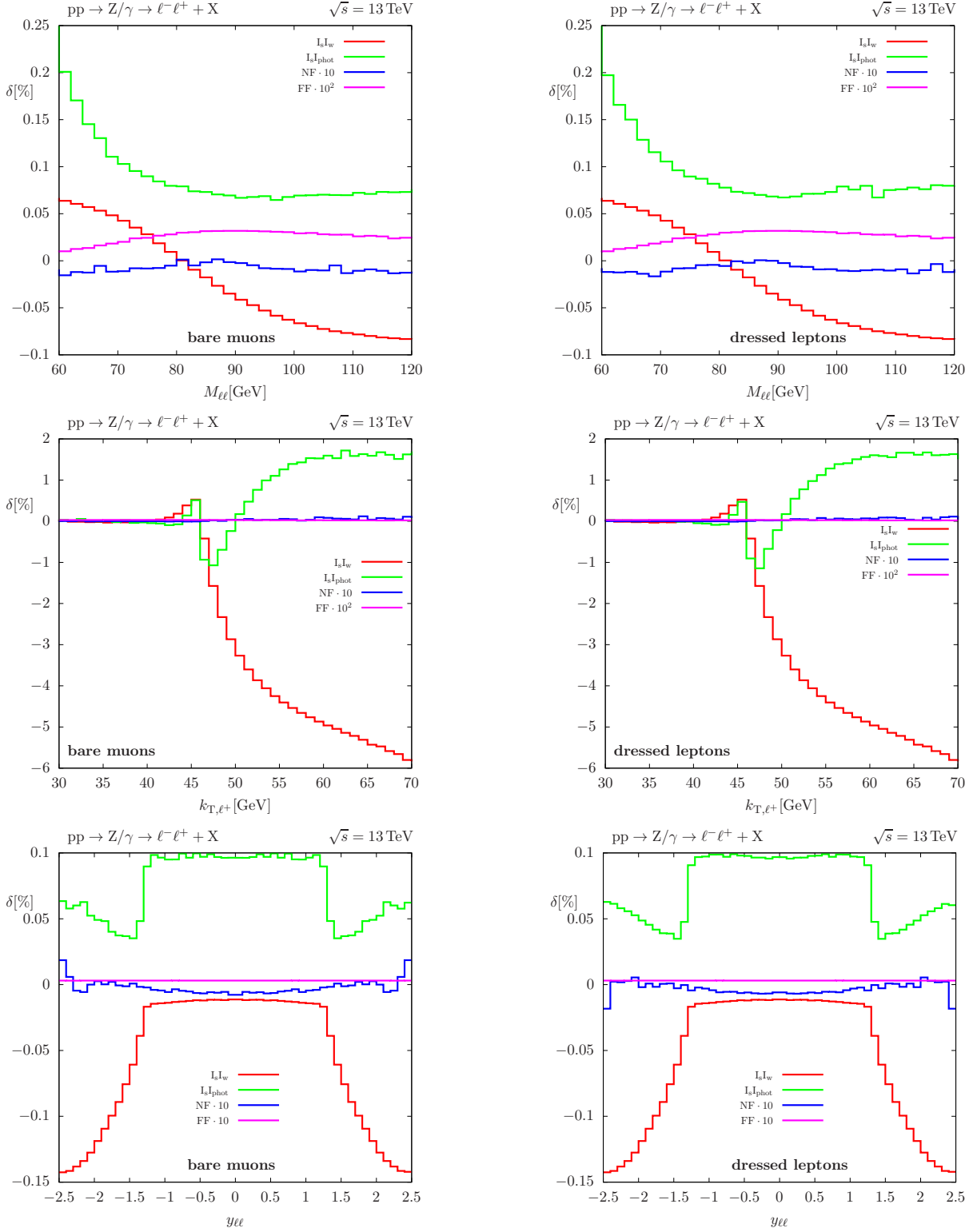


Figure 9: Subcontributions of the relative NNLO QCD  $\times$  EW corrections in PA (normalized to LO): II QCD  $\times$  weak (red), II QCD  $\times$  photonic (green), NF (blue), and FF QCD  $\times$  weak (magenta). The dominating IF contribution is contained in Fig. 8.

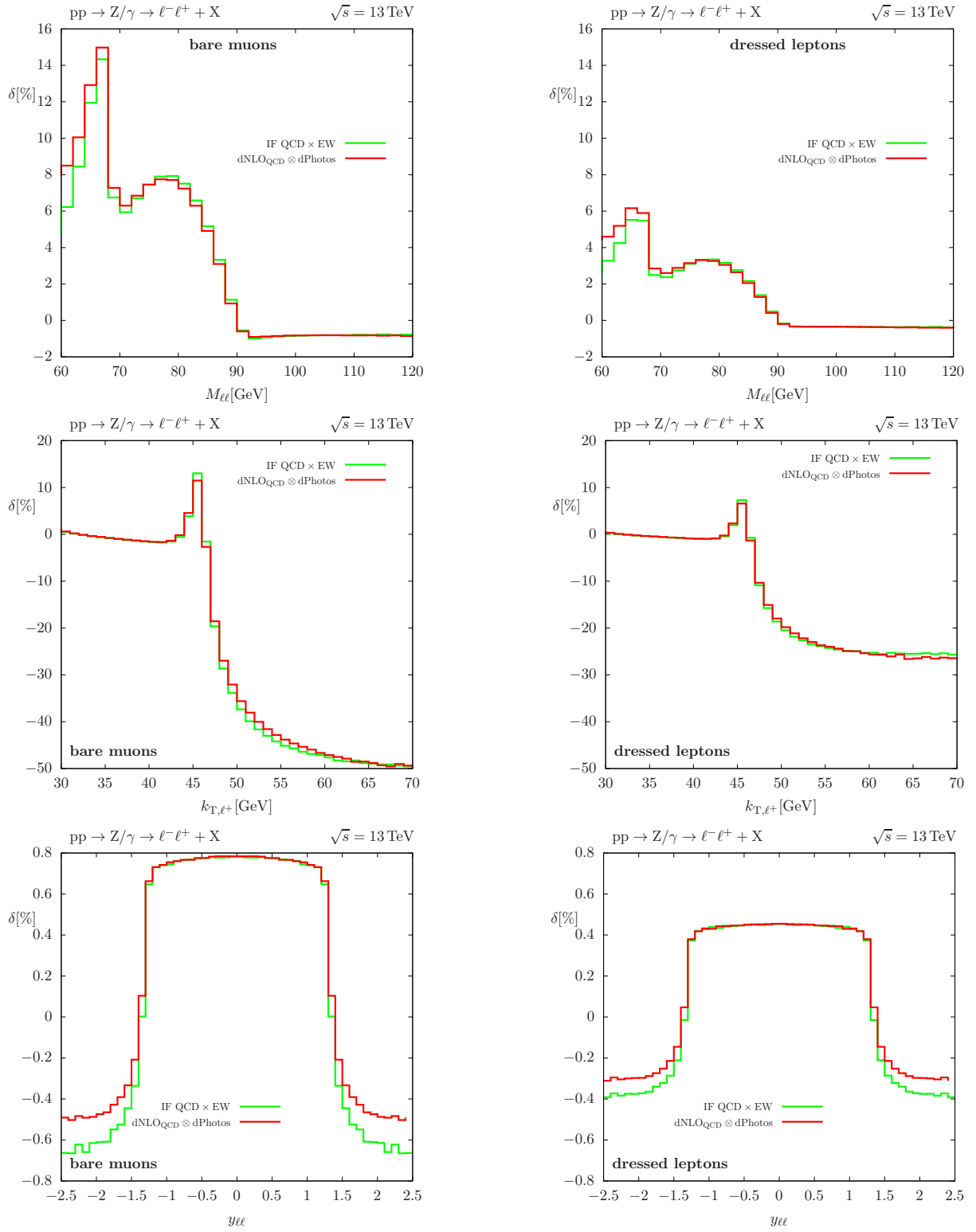


Figure 10: NNLO IF QCD  $\times$  EW (green) and dNLO<sub>QCD</sub>  $\otimes$  dPhotos (red) corrections, normalized to LO.

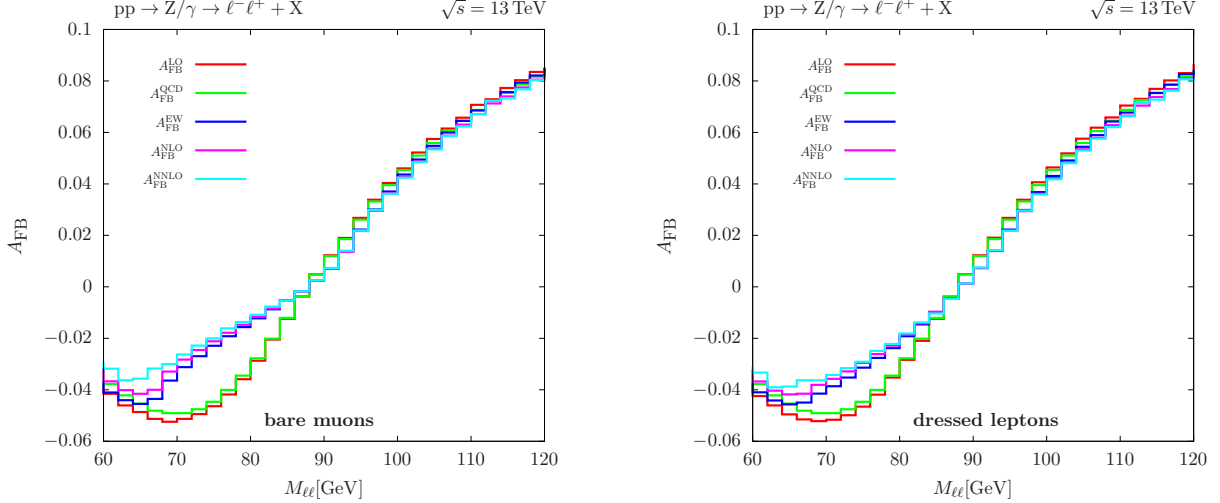


Figure 11: FB asymmetry  $A_{\text{FB}}$  for muon pair (left) and dressed-lepton pair (right) production at LO (red) and including various corrections: NLO QCD (green), NLO EW (blue), full NLO QCD + EW (pink), and NNLO  $\equiv$  NLO + EWHO +  $\Delta\text{LLFSR}$  + QCD $\times$ QCD + QCD $\times$ EW (light blue).

i.e.  $M_{\ell\ell}^2 = k_{\ell\ell}^2$ . All four-momenta are defined in the LAB frame.

The FB asymmetry  $A_{\text{FB}}(M_{\ell\ell})$  is mainly relevant for determining the leptonic effective weak mixing angle  $\sin^2\theta_{\text{w,eff}}^\ell$  defined on the Z resonance from an  $M_{\ell\ell}$  window around  $M_Z$  with a width of about  $\sim \pm 10$  GeV. LEP/SLC precision in  $\sin^2\theta_{\text{w,eff}}^\ell$  roughly translates into an uncertainty of  $\sim 10^{-3}$  in  $A_{\text{FB}}$ , so that the precision target for an improved determination of  $\sin^2\theta_{\text{w,eff}}^\ell$  at the LHC requires to control the prediction of  $A_{\text{FB}}(M_{\ell\ell})$  at the level of few  $\sim 10^{-4}$  in the vicinity of the Z resonance. Existing measurements of  $A_{\text{FB}}$  at the LHC [11, 12, 14, 120] are already at the accuracy level of  $10^{-3}$  near the Z resonance. Increased statistics from higher luminosity and steady improvements in the determination of parton distribution functions will tackle two of the main sources of uncertainties in these measurements, further challenging the precision of the underlying theory predictions.

In Fig. 11 the LO prediction for the FB asymmetry  $A_{\text{FB}}$  is compared to predictions including NLO QCD, NLO EW, and all available NNLO corrections, where

$$A_{\text{FB}}^x = \frac{\sigma_{\text{F}}^x - \sigma_{\text{B}}^x}{\sigma_{\text{F}}^x + \sigma_{\text{B}}^x}, \quad x = \text{LO, NLO, NNLO}, \quad (3.10)$$

where  $\sigma_{\text{F/B}}^x$  are the forward/backward cross sections (3.7) evaluated at order  $x$ . The absolute prediction for  $A_{\text{FB}}(M_{\ell\ell})$ , which is shown in Fig. 11, is of the order of  $10^{-2}$  near the Z resonance, and the impact of NLO and NNLO corrections is already visible there. To quantify the impact of the various corrections better, we consider the shifts with respect to the LO asymmetry:

$$\Delta A_{\text{FB}}^x = A_{\text{FB}}^{\text{LO}+\delta^x} - A_{\text{FB}}^{\text{LO}}, \quad (3.11)$$

where  $\delta^x$  indicates the higher-order correction of type  $x$ .

Figure 12 separately shows the impact of NLO QCD, NLO EW,  $\gamma$ -induced, and the pure photonic FSR part of the NLO EW corrections. The latter constitutes the dominat-

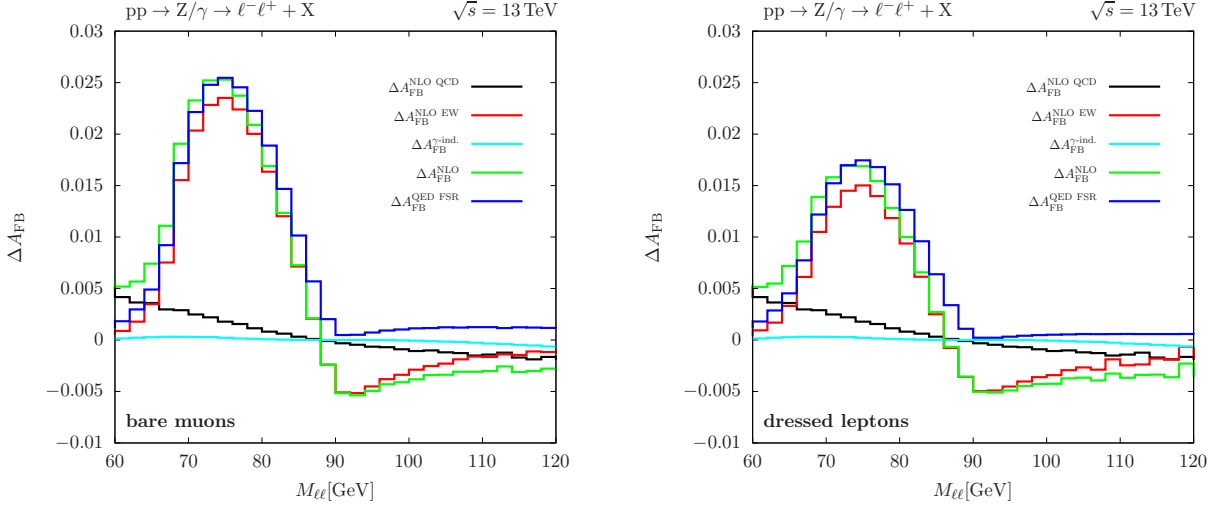


Figure 12: NLO corrections to the FB asymmetry  $A_{\text{FB}}$  for muon pair (left) and dressed-lepton pair (right) production: NLO QCD (black), NLO EW (red),  $\gamma$ -induced contribution (cyan), full NLO QCD + EW (green), and photonic FSR at NLO (blue).

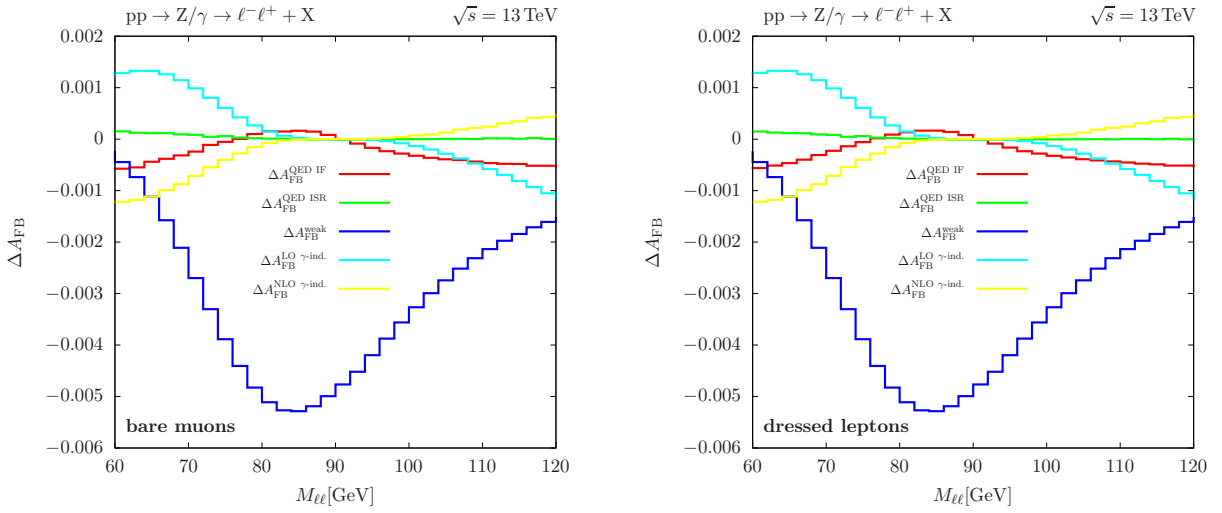


Figure 13: NLO EW corrections to the FB asymmetry  $A_{\text{FB}}$  for muon pair (left) and dressed-lepton pair (right) production induced by QED IF (red), QED ISR (green), and purely weak (blue) corrections, as well as contributions from LO  $\gamma\gamma$  (cyan) and NLO  $q\gamma/\bar{q}\gamma$  (yellow) initial states.

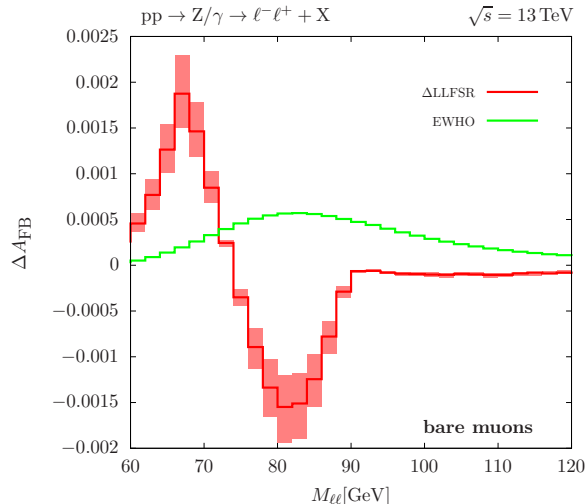


Figure 14: NNLO  $\Delta$ LLFSR (red) and EWHO corrections to the forward–backward asymmetry. Within the red band the scale  $\mu = \mu_F = \mu_R$  is varied in the calculation of the LLFSR corrections in the range  $M_Z/2 < \mu < 2M_Z$ .

ing effect with an impact of  $\sim 10^{-2}$  at the edge of the  $M_Z - 10 \text{ GeV} < M_{\ell\ell} < M_Z + 10 \text{ GeV}$  window around the Z resonance. NLO QCD corrections are in the ballpark of  $\sim 10^{-3}$ , while the photon-induced contributions are strongly suppressed as expected. The NLO EW corrections not connected to FSR are illustrated in Fig. 13 together with the separation of the  $\gamma$ -induced contributions into LO and NLO parts. After the FSR effects, the most prominent contribution at NLO EW is given by the purely weak corrections, which reach up to  $5 \times 10^{-3}$ . The photonic IF interference, photonic ISR, and  $\gamma$ -induced effects typically contribute only fractions of  $10^{-3}$ , but have to be taken into account in predictions at the targeted level of precision. We note that the LO  $\gamma\gamma$  contribution is symmetric in the forward and backward directions, however, the change in the (symmetric) denominator of Eq. (3.10) gives rise to a non-vanishing effect in Eq. (3.11) seen in the figures.

Figure 14 shows the effect of multi-photon emission off leptons and of the universal higher-order EW corrections beyond NLO on the FB asymmetry. The higher-order FSR corrections modify  $A_{\text{FB}}$  at the level of  $\sim 10^{-3}$  with a residual scale uncertainty of a few  $10^{-4}$  and are, thus, important. On the other hand, the NNLO universal EW corrections amount only to a few  $10^{-4}$ .

In Fig. 15 we contrast full NLO EW corrections and QED FSR effects with a prediction based on the PHOTOS QED shower on top of the LO prediction. We see good agreement between FSR corrections and the QED shower and the small normalization difference that was observed in the absolute predictions of Fig. 7 largely drop out in the observable  $A_{\text{FB}}$ . A notable difference to the absolute predictions discussed in the previous section is the much more pronounced impact of non-FSR effects as can be assessed from a comparison to the full NLO EW curve. This does not come as a surprise given the strong sensitivity of this observable to the weak sector of the Standard Model.

In Fig. 16 we show the impact of the NNLO QCD and QCD  $\times$  EW corrections in PA, together with the dominating IF contribution of the latter. The QCD  $\times$  EW IF corrections

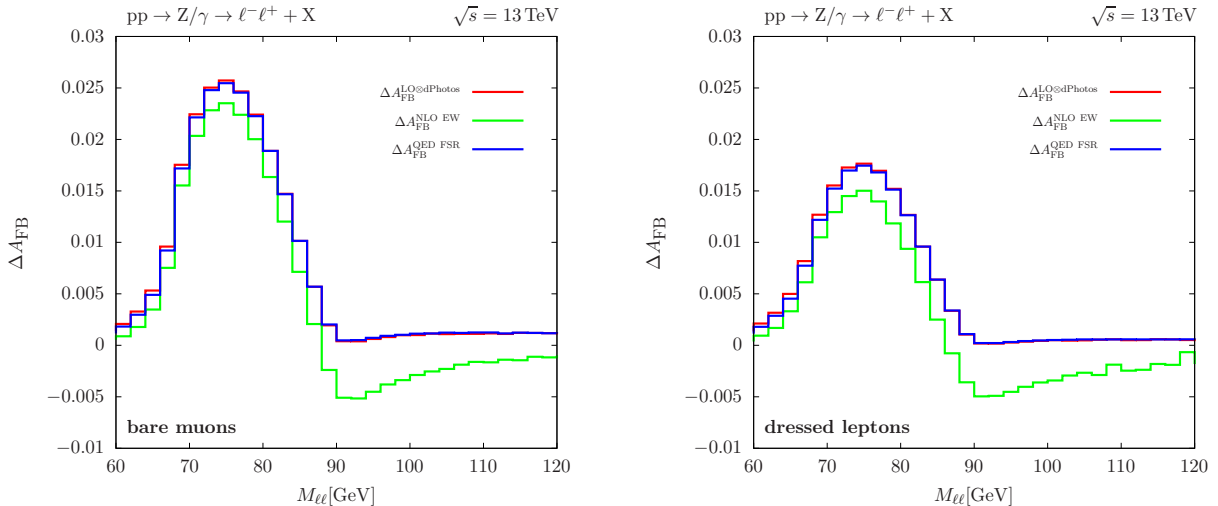


Figure 15: NLO EW (green) and LO  $\otimes$  dPhotos (red) corrections to the FB asymmetry.

change the FB asymmetry in the vicinity of the Z resonance by a few  $10^{-3}$  and are, thus, phenomenologically very important, while the NNLO QCD corrections contribute only at the level of few  $10^{-4}$ . The QCD  $\times$  EW corrections of types other than IF are depicted in Fig. 17. While the corrections of type FF still reach the relevant level of  $4 \times 10^{-4}$ , the QCD  $\times$  photonic and QCD  $\times$  weak II corrections as well as the NF contributions are well below  $10^{-4}$  and, thus, phenomenologically negligible.

Finally, Figure 18 shows the comparison of the results obtained with the QED shower PHOTOS on top of the NLO QCD prediction,  $\text{dNLO}_{\text{QCD}} \otimes \text{PHOTOS}$ , with the IF factorizable  $\mathcal{O}(\alpha_s\alpha)$  corrections. A similar picture emerges here as at the previous order where the agreement between the two results that was seen in the absolute predictions of Fig. 10 substantially degrades in this observable, with a notable shape distortion that pivots around the resonance. This is again likely due to the more sizeable impact of the non-FSR contributions that are not captured by a QED shower.

## 4 Summary

Next-to-next-to-leading-order (NNLO) corrections of mixed QCD  $\times$  electroweak (EW) origin, together with the recent process in third-order ( $\text{N}^3\text{LO}$ ) QCD results, are among the most important fixed-order corrections beyond the well-known NNLO QCD and next-to-leading-order (NLO) EW corrections to differential cross sections of Drell–Yan-like lepton pair production. In the vicinity of the Z-boson resonance, the pole approximation (PA) can be used to reduce the complexity of the NNLO QCD  $\times$  EW corrections significantly. The PA allows to classify the corrections into four separately gauge-invariant building blocks: corrections of types initial–initial (II), initial–final (IF), final–final (FF), and non-factorizable (NF) corrections. Making use of previous calculations of the IF, FF, and NF corrections, in this paper we have completed the PA at the order  $\mathcal{O}(\alpha_s\alpha)$  by calculating the corrections of type II.

Technically, we have split the  $\mathcal{O}(\alpha_s\alpha)$  II corrections of the PA into two separately gauge-invariant parts: the QCD  $\times$  photonic corrections with photon exchange between

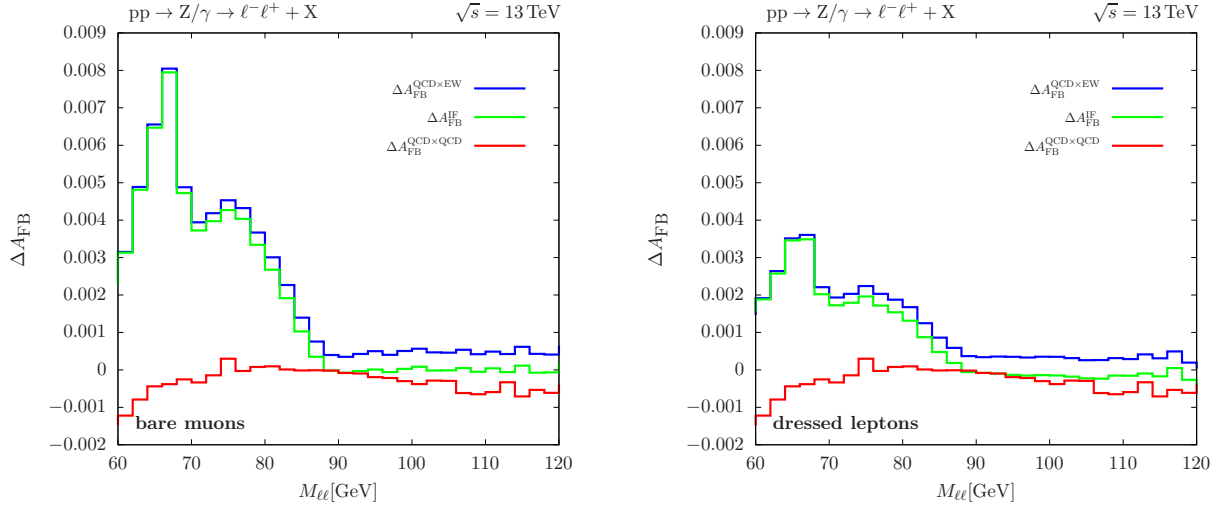


Figure 16: NNLO  $\text{QCD} \times \text{QCD}$  corrections (red), full  $\text{QCD} \times \text{EW}$  corrections in PA (blue), and IF  $\text{QCD} \times \text{EW}$  corrections in PA (green) to the FB asymmetry.

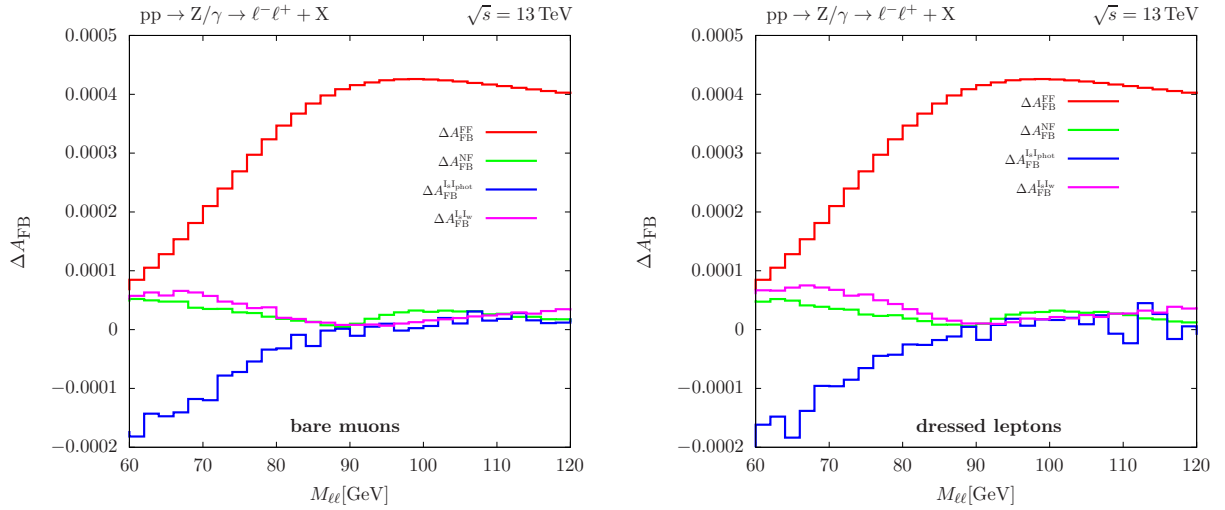


Figure 17: NNLO  $\text{QCD} \times \text{EW}$  corrections of types FF (red), NF (green),  $I_s I_p$  (blue), and  $I_s I_w$  (purple) to the FB asymmetry.

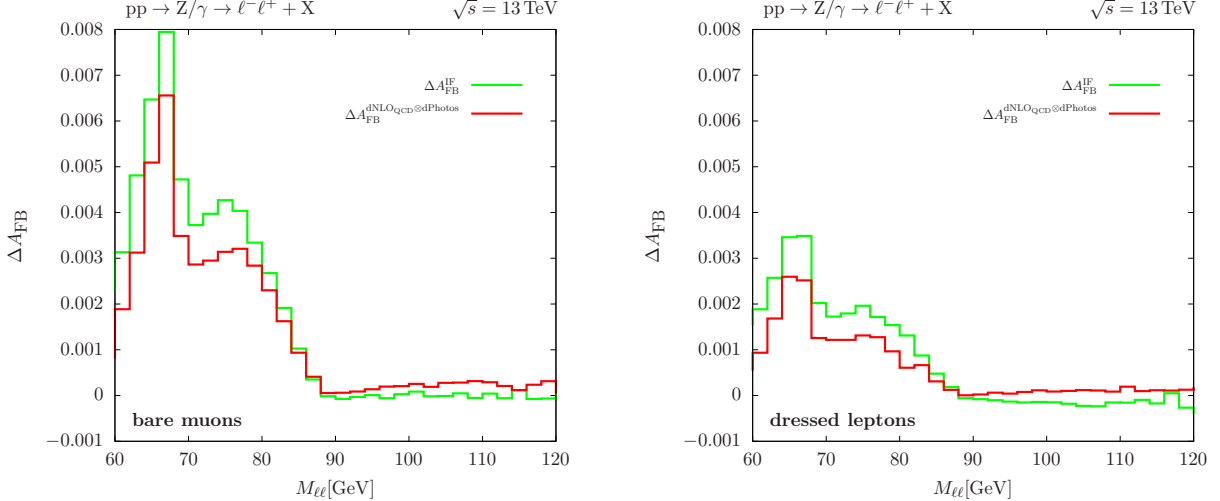


Figure 18: NNLO IF QCD  $\times$  EW (green) and dNLO<sub>QCD</sub>  $\otimes$  dPhotos (red) corrections to the FB asymmetry.

and photon radiation off quarks, which we have evaluated without using the PA, and the QCD  $\times$  weak corrections with additional W/Z exchange in loops in PA. For the latter, we have recalculated the needed two-loop  $Z\bar{q}q$  formfactor and presented explicit analytical results. For the QCD infrared (IR) singularities, which are only of NLO complexity in this part, we have applied antenna and dipole subtraction. The IR singularities of the QCD  $\times$  photonic corrections, which are of NNLO complexity, are treated with antenna subtraction. All our results have been derived in two completely independent calculations, the results of which are in good mutual numerical agreement.

Although the  $\mathcal{O}(\alpha_s\alpha)$  corrections to the full off-shell lepton pair production process have been calculated in recent years, the completion of the PA is still very useful. Firstly, a detailed numerical comparison between the full calculation and the PA sheds light on the structure of the  $\mathcal{O}(\alpha_s\alpha)$  corrections, which might be helpful in calculating or approximating such corrections for related processes. The completion of the PA presented here renders such a comparison possible. Secondly, the full off-shell calculation is extremely complex and numerically challenging. For this reason, a detailed discussion of the  $\mathcal{O}(\alpha_s\alpha)$  corrections to the forward-backward asymmetry  $A_{\text{FB}}$  of the leptons that is fully differential wrt. the invariant mass of the lepton pair was still missing in the literature. With the numerical results presented in this paper we have closed this gap.

The prospects to measure the leptonic effective weak mixing angle in the high-luminosity phase of the LHC with a precision exceeding LEP accuracy, translates into a target precision in the predictions for  $A_{\text{FB}}$  of a few  $10^{-4}$  in the Z resonance region. We have presented a detailed survey of higher-order corrections, comprising results at the NLO QCD + EW level, the NNLO QCD + QCD  $\times$  EW level, and leading EW effects beyond NLO from multi-photon emission and universal EW corrections. Photonic final-state radiation (FSR) at NLO produces the largest correction to  $A_{\text{FB}}$  of about  $10^{-2}$ , followed by the NLO weak corrections of about  $5 \times 10^{-3}$ . The remaining NLO contributions, including QCD, affect  $A_{\text{FB}}$  at the level of few  $10^{-3}$ . The NNLO  $\mathcal{O}(\alpha_s\alpha)$  corrections of IF type, which combine QCD corrections to Z production and photonic FSR off the



leptons modify  $A_{\text{FB}}$  at the level of few  $1-2 \times 10^{-3}$ , which is also the typical size of multi-photon effects. Finally, the NNLO QCD corrections and the remaining  $\mathcal{O}(\alpha_s\alpha)$  corrections generically matter at the level of a few  $10^{-4}$ .

As already mentioned, one of the natural next steps in the evaluation of  $\mathcal{O}(\alpha_s\alpha)$  corrections to Drell–Yan-like processes is a detailed comparison of PA-based and full off-shell results for all individual ingredients, such as photonic and weak corrections to lepton pair production. Last but not least, another important step will be the completion of both the PA and the full off-shell calculation of  $\mathcal{O}(\alpha_s\alpha)$  corrections to the charged-current process of W production, which will be particularly important for upcoming high-precision measurements of the W-boson mass at the LHC.

## Acknowledgements

We thank Timo Schmidt for contributions in the calculation of integrals in an early stage of this work. SD and JS acknowledge support by the state of Baden-Württemberg through bwHPC and the German Research Foundation (DFG) through grants no. INST 39/963-1 FUGG, grant DI 785/1, and the DFG Research Training Group RTG2044.

## Appendix

### A Formfactors for the irreducible $\mathcal{O}(\alpha_s\alpha_w)$ corrections to the $Z\bar{f}f$ vertex

Here we present our explicit analytical results for the formfactor functions  $\phi_A(z)$  and  $\phi_{\text{NA}}(z)$  defined in Ref. [81] to describe the irreducible contributions of  $\mathcal{O}(\alpha_s\alpha_w)$  to the  $Z\bar{f}f$  vertex corrections, as defined in Eq. (2.10). These contributions correspond to the difference between the full formfactors and the naive product of the corresponding  $\mathcal{O}(\alpha_s)$  QCD and  $\mathcal{O}(\alpha_w)$  weak contributions. We prefer to call those parts “irreducible” rather than “non-factorizable” (as done in Ref. [81]) to avoid confusion with our classification of the different types of corrections arising in the resonance expansion.

We have performed a completely independent recalculation of the formfactors employing standard methods. In detail, we have generated the two-loop graphs with FEYNARTS 1.0 [89] and further algebraically processed the amplitudes with inhouse MATHEMATICA routines, to express them in terms of scalar two-loop integrals. The large set of two-loop integrals is reduced to a set of master integrals with Laporta’s algorithm [121], employing the program KIRA 2.0 [90, 122]. Finally, the master integrals are calculated via differential equations using Henn’s canonical  $\epsilon$ -form [92, 93], directly producing a result in terms of Goncharov Polylogarithms (GPLs) [94, 95].

For the formfactor functions  $\phi_A(z)$  and  $\phi_{\text{NA}}(z)$  of Ref. [81] we explicitly get

$$\begin{aligned}
\phi_A(z) = & \frac{4(1+z)^2}{3z^2} \left[ -24G(0, 1, 0, -1; -z) + 6G(0, 1, 0, 0; -z) - 6G(1, 0, 0, -1; -z) \right. \\
& - 12G(1, 0, 1, 0; -z) + 36G(1, 1, 0, -1; -z) - 12G(1, 1, 0, 0; -z) \\
& + 12G(1, 1, 1, 0; -z) - 18G(1, 0, -1; -z) + 9G(1, 0, 0; -z) \\
& - 9G(1, 1, 0; -z) + 2\pi^2 G(0, 1; -z) - 5\pi^2 G(1, 1; -z) \\
& \left. - 3(6\zeta_3 - \pi^2)G(1; -z) \right] \\
& + \frac{16(1+3z+z^2)}{3z^2} \left[ -3G(0, -1, 0, -1; -z) + 3G(0, -1, 0, 0; -z) \right. \\
& \left. + \pi^2 G(0, -1; -z) \right] \\
& + \frac{12(1-z^2)}{z^2} \left[ \pi^2 G(-1; -z) - 3G(-1, 0, -1; -z) + 3G(-1, 0, 0; -z) \right] \\
& + \frac{(2+3z)}{3z} \left[ 12G(0, 1, 0; -z) + 36\zeta_3 + 16\pi^2 - 51G(0; -z) \right] \\
& + \frac{4(4+3z)}{z} G(0, 0, -1; -z) - \frac{4(11+9z)}{z} G(0, -1; -z) \\
& + \frac{2(16+23z)}{z} G(0, 0; -z) - \frac{2(1+z)(3+5z)}{z^2} G(1, 0; -z) \\
& + \frac{2(-1+z)(13+27z)}{z^2} G(-1; -z) - 2 + \frac{16}{z}, \tag{A.1}
\end{aligned}$$

$$\begin{aligned}
\phi_{\text{NA}}(z) = & \frac{8(1+z)^2}{3z^2} \left[ 6G(0, -1, 0, -1; -z) - 6G(0, -1, 0, 0; -z) + 24G(0, 1, 0, -1; -z) \right. \\
& \left. - 6G(0, 1, 0, 0; -z) + 6G(1, 0, 0, -1; -z) + 12G(1, 0, 1, 0; -z) \right]
\end{aligned}$$

$$\begin{aligned}
& - 36G(1, 1, 0, -1; -z) + 12G(1, 1, 0, 0; -z) - 12G(1, 1, 1, 0; -z) \\
& + 18\zeta_3 G(1; -z) + 5\pi^2 G(1, 1; -z) + 18G(1, 0, -1; -z) - 9G(1, 0, 0; -z) \\
& + 9G(1, 1, 0; -z) - 3\pi^2 G(1; -z) - 2\pi^2 G(0, -1; -z) - 2\pi^2 G(0, 1; -z) \Big] \\
& + \frac{8(1-z^2)}{z^2} \left[ 3G(-1, 0, -1; -z) - 3G(-1, 0, 0; -z) - \pi^2 G(-1; -z) \right] \\
& - \frac{8(4+3z)}{z} G(0, 0, -1; -z) - \frac{8(2+3z)}{z} G(0, 1, 0; -z) \\
& - \frac{4(1+3z)(5+3z)}{z^2} G(0, -1; -z) + \frac{4(1+z)(3+5z)}{z^2} G(1, 0; -z) \\
& - \frac{4(1-z)(13+19z)}{z^2} G(-1; -z) - \frac{6(2+7z)}{z} G(0; -z) \\
& - \frac{48(1-y^2)(1-2y)}{y^4} \left[ 2G(0, 1, 1, 1; y) - 2G(0, 1, 1, y_2; y) - 2G(0, 1, 1, y_1; y) \right. \\
& \quad \left. - G(1, 1, 1, 1; y) + G(1, 1, 1, y_2; y) + G(1, 1, 1, y_1; y) \right] \\
& - 16G(0, 0, 1; y) + 16G(0, 0, y_2; y) + 16G(0, 0, y_1; y) + 24G(0, 1, 1; y) \\
& - 8G(0, 1, y_2; y) - 8G(0, 1, y_1; y) + 8G(1, 0, 1; y) - 8G(1, 0, y_2; y) \\
& - 8G(1, 0, y_1; y) - 8G(1, 1, y_2; y) - 8G(1, 1, y_1; y) \\
& - \frac{4(10-20y-4y^2+14y^3+5y^4)}{y^4} \left[ G(0, 1; y) - G(0, y_2; y) - G(0, y_1; y) \right] \\
& - \frac{4(-11+34y-20y^2-12y^3+5y^4)}{y^4} G(1, 1; y) \\
& + \frac{4(-5+22y-16y^2-10y^3+2y^4)}{y^4} \left[ G(1, y_2; y) + G(1, y_1; y) \right] \\
& + \frac{2(-26+64y-46y^2-6y^3+31y^4)}{y^4} G(1; y) \\
& - \frac{4(1-y+y^2)(-13+13y+12y^2)}{y^4} \left[ G(y_2; y) + G(y_1; y) \right] \\
& - \frac{48\zeta_3}{z} - 72\zeta_3 - \frac{4\pi^2}{3} - \frac{60}{y^2} + \frac{60}{y} - \frac{60}{z} - 16, \tag{A.2}
\end{aligned}$$

where

$$\begin{aligned}
z &= \frac{q^2}{M^2} + i0, & y_{1,2} &= \frac{1}{2}(1 \pm i\sqrt{3}), \\
y = y(z) &= \begin{cases} [z - \sqrt{z(z-4)}]/2 & \text{for } q^2 < 0, \\ 2z/[z + \sqrt{z(z-4)}] & \text{for } q^2 > 4M^2, \\ [z - i\sqrt{z(4-z)}]/2 & \text{otherwise.} \end{cases} \tag{A.3}
\end{aligned}$$

The variable  $y$  is a solution of the quadratic equation  $0 = z(1-y) + y^2$  with the special property that the contour from  $y(0) = 0$  to  $y(z)$  defined by  $z = r + i0$ ,  $r \in \mathbb{R}$ , is homotopic to the straight line from 0 to  $y(r+i0)$  in the complex  $y$  plane going between the singularities at  $y_{1,2}$  without hitting them. This property guarantees the correct analytical

	our result	Ref. [81]
$\phi_A(1 + i0)$	$-2.1073169 - 19.033126i$	$-2.1073 - 19.0331i$
$\phi_{NA}(1 + i0)$	$-7.5879998 + 16.719365i$	$-7.5880 + 16.7194i$
$\phi_A(1.2856 + i0)$	$-1.3610142 - 22.238253i$	$-1.3598 - 30.4095i$
$\phi_{NA}(1.2856 + i0)$	$-10.121177 + 18.696957i$	$-10.1248 + 35.0336i$

Table 1: Comparison our numerical results on  $\phi_A(z)$  and  $\phi_{NA}(z)$  with the benchmark numbers given in Ref. [81].

behaviour when integrating the differential equations in the kinematical variable  $y$  via straight lines as contours in the complex  $y$  plane with  $y = 0$  ( $q^2 = 0$ ) as start condition. This directly leads to GPLs in  $y$ , without picking up contributions from residues resulting from contour deformations. Note that  $y(1) = y_2$  lies on the curve  $y(r)$  with  $r \in \mathbb{R}$  which is obtained without taking Feynman’s  $i0$  prescription into account, and the  $i0$  prescription circumvents  $y_2$  in the “correct direction”. A similar path defined from the second solution of  $0 = z(1 - y) + y^2$  would circumvent  $y_1$  in the “wrong direction”, so that a path defined analogously to the above  $y(z)$  would not be homotopic to the straight line from 0 to  $y(r + i0)$ .

Since a direct comparison of our analytical results for  $\phi_A(z)$  and  $\phi_{NA}(z)$  to the ones given in Ref. [81] seems too cumbersome, we have compared those functions numerically for the benchmark points given in Ref. [81]. The results of this comparison is shown in Tab. 1. While our results confirm the ones given in Ref. [81] for  $z = 1 + i0$  for all digits given there, we find significant differences for  $z = 1.2856 + i0$ ; in particular, the imaginary parts of  $\phi_A(1.2856 + i0)$  and  $\phi_{NA}(1.2856 + i0)$  are totally different in the two evaluations. For this reason, we have implemented and numerically evaluated the analytical results of Ref. [81] as well. The corresponding third set of results completely confirms our results given in Tab. 1 to all digits given there. We therefore conclude that the analytical results of Ref. [81] are in fact in agreement with ours, but the benchmark numbers on  $\phi_A(1.2856 + i0)$  and  $\phi_{NA}(1.2856 + i0)$  given there are not correct.

## References

- [1] M. Dittmar, F. Pauss, and D. Zurcher, *Towards a precise parton luminosity determination at the CERN LHC*, *Phys. Rev. D* **56** (1997) 7284–7290, [hep-ex/9705004].
- [2] V. A. Khoze, A. D. Martin, R. Orava, and M. Ryskin, *Luminosity monitors at the LHC*, *Eur. Phys. J. C* **19** (2001) 313–322, [hep-ph/0010163].
- [3] **TeV4LHC Working Group** Collaboration, S. Abdullin et al., *Tevatron-for-LHC Report: Preparations for Discoveries*, 8, 2006. hep-ph/0608322.
- [4] **TeV4LHC-Top, Electroweak Working Group** Collaboration, C. Gerber et al., *Tevatron-for-LHC Report: Top and Electroweak Physics*, 5, 2007. arXiv:0705.3251.

- [5] S. Haywood et al., *Electroweak physics*, in *CERN Workshop on Standard Model Physics (and more) at the LHC (Final Plenary Meeting)*, pp. 117–230, 10, 1999. [hep-ph/0003275](#).
- [6] **CDF, D0** Collaboration, T. Aaltonen et al., *Combination of CDF and D0 W-Boson Mass Measurements*, *Phys. Rev. D* **88** (2013) 052018, [[arXiv:1307.7627](#)].
- [7] **ATLAS** Collaboration, M. Aaboud et al., *Measurement of the W-boson mass in pp collisions at  $\sqrt{s} = 7$  TeV with the ATLAS detector*, *Eur. Phys. J. C* **78** (2018) 110, [[arXiv:1701.07240](#)]. [Erratum: *Eur.Phys.J.C* 78, 898 (2018)].
- [8] **CDF** Collaboration, T. Aaltonen et al., *High-precision measurement of the W boson mass with the CDF II detector*, *Science* **376** (2022) 170–176.
- [9] **ATLAS** Collaboration, *Improved W boson Mass Measurement using 7 TeV Proton-Proton Collisions with the ATLAS Detector*, .
- [10] **CMS** Collaboration, S. Chatrchyan et al., *Measurement of the weak mixing angle with the Drell–Yan process in proton–proton collisions at the LHC*, *Phys. Rev. D* **84** (2011) 112002, [[arXiv:1110.2682](#)].
- [11] **ATLAS** Collaboration, G. Aad et al., *Measurement of the forward–backward asymmetry of electron and muon pair-production in pp collisions at  $\sqrt{s} = 7$  TeV with the ATLAS detector*, *JHEP* **09** (2015) 049, [[arXiv:1503.03709](#)].
- [12] **LHCb** Collaboration, R. Aaij et al., *Measurement of the forward–backward asymmetry in  $Z/\gamma^* \rightarrow \mu^+\mu^-$  decays and determination of the effective weak mixing angle*, *JHEP* **11** (2015) 190, [[arXiv:1509.07645](#)].
- [13] **CDF, D0** Collaboration, T. Aaltonen et al., *Tevatron Run II combination of the effective leptonic electroweak mixing angle*, *Phys. Rev. D* **97** (2018) 112007, [[arXiv:1801.06283](#)].
- [14] **CMS** Collaboration, A. Sirunyan et al., *Measurement of the weak mixing angle using the forward–backward asymmetry of Drell–Yan events in pp collisions at 8 TeV*, *Eur. Phys. J. C* **78** (2018) 701, [[arXiv:1806.00863](#)].
- [15] M. Boonekamp, F. Chevallier, C. Royon, and L. Schoeffel, *Understanding the Structure of the Proton: From HERA and Tevatron to LHC*, *Acta Phys. Polon. B* **40** (2009) 2239–2321, [[arXiv:0902.1678](#)].
- [16] R. Hamberg, W. van Neerven, and T. Matsuura, *A complete calculation of the order  $\alpha_s^2$  correction to the Drell-Yan K factor*, *Nucl. Phys. B* **359** (1991) 343–405. [Erratum: *Nucl.Phys.B* 644, 403–404 (2002)].
- [17] R. Gavin, Y. Li, F. Petriello, and S. Quackenbush, *W Physics at the LHC with FEWZ 2.1*, *Comput. Phys. Commun.* **184** (2013) 208–214, [[arXiv:1201.5896](#)].

- [18] R. Gavin, Y. Li, F. Petriello, and S. Quackenbush, *FEWZ 2.0: A code for hadronic Z production at next-to-next-to-leading order*, *Comput. Phys. Commun.* **182** (2011) 2388–2403, [[arXiv:1011.3540](#)].
- [19] S. Catani et al., *Vector boson production at hadron colliders: a fully exclusive QCD calculation at NNLO*, *Phys. Rev. Lett.* **103** (2009) 082001, [[arXiv:0903.2120](#)].
- [20] K. Melnikov and F. Petriello, *Electroweak gauge boson production at hadron colliders through  $O(\alpha_s^2)$* , *Phys. Rev. D* **74** (2006) 114017, [[hep-ph/0609070](#)].
- [21] K. Melnikov and F. Petriello, *The W boson production cross section at the LHC through  $O(\alpha_s^2)$* , *Phys. Rev. Lett.* **96** (2006) 231803, [[hep-ph/0603182](#)].
- [22] C. Anastasiou, L. J. Dixon, K. Melnikov, and F. Petriello, *High precision QCD at hadron colliders: Electroweak gauge boson rapidity distributions at NNLO*, *Phys. Rev. D* **69** (2004) 094008, [[hep-ph/0312266](#)].
- [23] R. V. Harlander and W. B. Kilgore, *Next-to-next-to-leading order Higgs production at hadron colliders*, *Phys. Rev. Lett.* **88** (2002) 201801, [[hep-ph/0201206](#)].
- [24] C. Duhr, F. Dulat, and B. Mistlberger, *Drell-Yan Cross Section to Third Order in the Strong Coupling Constant*, *Phys. Rev. Lett.* **125** (2020) 172001, [[arXiv:2001.07717](#)].
- [25] C. Duhr and B. Mistlberger, *Lepton-pair production at hadron colliders at  $N^3LO$  in QCD*, *JHEP* **03** (2022) 116, [[arXiv:2111.10379](#)].
- [26] J. Baglio, C. Duhr, B. Mistlberger, and R. Szafron, *Inclusive production cross sections at  $N^3LO$* , *JHEP* **12** (2022) 066, [[arXiv:2209.06138](#)].
- [27] X. Chen, et al., *Dilepton Rapidity Distribution in Drell-Yan Production to Third Order in QCD*, *Phys. Rev. Lett.* **128** (2022) 052001, [[arXiv:2107.09085](#)].
- [28] X. Chen, et al., *Transverse mass distribution and charge asymmetry in W boson production to third order in QCD*, *Phys. Lett. B* **840** (2023) 137876, [[arXiv:2205.11426](#)].
- [29] X. Chen, et al., *Third-Order Fiducial Predictions for Drell-Yan Production at the LHC*, *Phys. Rev. Lett.* **128** (2022) 252001, [[arXiv:2203.01565](#)].
- [30] T. Neumann and J. Campbell, *Fiducial Drell-Yan production at the LHC improved by transverse-momentum resummation at  $N_4LLp+N_3LO$* , *Phys. Rev. D* **107** (2023) L011506, [[arXiv:2207.07056](#)].
- [31] M. Guzzi, P. M. Nadolsky, and B. Wang, *Nonperturbative contributions to a resummed leptonic angular distribution in inclusive neutral vector boson production*, *Phys. Rev. D* **90** (2014) 014030, [[arXiv:1309.1393](#)].
- [32] A. Kulesza and W. Stirling, *Soft gluon resummation in transverse momentum space for electroweak boson production at hadron colliders*, *Eur. Phys. J. C* **20** (2001) 349–356, [[hep-ph/0103089](#)].

- [33] S. Catani, D. de Florian, G. Ferrera, and M. Grazzini, *Vector boson production at hadron colliders: transverse-momentum resummation and leptonic decay*, *JHEP* **12** (2015) 047, [[arXiv:1507.06937](#)].
- [34] C. Balazs and C. Yuan, *Soft gluon effects on lepton pairs at hadron colliders*, *Phys. Rev. D* **56** (1997) 5558–5583, [[hep-ph/9704258](#)].
- [35] F. Landry, R. Brock, P. M. Nadolsky, and C. Yuan, *Tevatron Run-1 Z boson data and Collins-Soper-Sterman resummation formalism*, *Phys. Rev. D* **67** (2003) 073016, [[hep-ph/0212159](#)].
- [36] G. Bozzi et al., *Production of Drell-Yan lepton pairs in hadron collisions: Transverse-momentum resummation at next-to-next-to-leading logarithmic accuracy*, *Phys. Lett. B* **696** (2011) 207–213, [[arXiv:1007.2351](#)].
- [37] S. Mantry and F. Petriello, *Transverse Momentum Distributions from Effective Field Theory with Numerical Results*, *Phys. Rev. D* **83** (2011) 053007, [[arXiv:1007.3773](#)].
- [38] T. Becher, M. Neubert, and D. Wilhelm, *Electroweak Gauge-Boson Production at Small  $q_T$ : Infrared Safety from the Collinear Anomaly*, *JHEP* **02** (2012) 124, [[arXiv:1109.6027](#)].
- [39] W. Bizoń, et al., *Fiducial distributions in Higgs and Drell-Yan production at  $N^3LL+NNLO$* , *JHEP* **12** (2018) 132, [[arXiv:1805.05916](#)].
- [40] W. Bizon, et al., *The transverse momentum spectrum of weak gauge bosons at  $N^3LL+NNLO$* , *Eur. Phys. J. C* **79** (2019) 868, [[arXiv:1905.05171](#)].
- [41] E. Re, L. Rottoli, and P. Torrielli, *Fiducial Higgs and Drell-Yan distributions at  $N^3LL+NNLO$  with RadISH*, [arXiv:2104.07509](#).
- [42] W.-L. Ju and M. Schönherr, *The  $q_T$  and  $\Delta\phi$  spectra in W and Z production at the LHC at  $N^3LL'+N^2LO$* , *JHEP* **10** (2021) 088, [[arXiv:2106.11260](#)].
- [43] S. Camarda, L. Cieri, and G. Ferrera, *Drell-Yan lepton-pair production:  $q_T$  resummation at  $N^3LL$  accuracy and fiducial cross sections at  $N^3LO$* , *Phys. Rev. D* **104** (2021) L111503, [[arXiv:2103.04974](#)].
- [44] T. Ahmed, M. Mahakhud, N. Rana, and V. Ravindran, *Drell-Yan Production at Threshold to Third Order in QCD*, *Phys. Rev. Lett.* **113** (2014) 112002, [[arXiv:1404.0366](#)].
- [45] S. Catani et al., *Threshold resummation at  $N^3LL$  accuracy and soft-virtual cross sections at  $N^3LO$* , *Nucl. Phys. B* **888** (2014) 75–91, [[arXiv:1405.4827](#)].
- [46] U. Baur, S. Keller, and W. Sakumoto, *QED radiative corrections to Z boson production and the forward backward asymmetry at hadron colliders*, *Phys. Rev. D* **57** (1998) 199–215, [[hep-ph/9707301](#)].

- [47] V. Zykunov, *Electroweak corrections to the observables of W boson production at RHIC*, *Eur. Phys. J. direct* **3** (2001) 9, [[hep-ph/0107059](#)].
- [48] U. Baur et al., *Electroweak radiative corrections to neutral current Drell-Yan processes at hadron colliders*, *Phys. Rev. D* **65** (2002) 033007, [[hep-ph/0108274](#)].
- [49] S. Dittmaier and M. Krämer, *Electroweak radiative corrections to W boson production at hadron colliders*, *Phys. Rev. D* **65** (2002) 073007, [[hep-ph/0109062](#)].
- [50] U. Baur and D. Wackerroth, *Electroweak radiative corrections to  $p\bar{p} \rightarrow W^\pm \rightarrow \ell^\pm \nu$  beyond the pole approximation*, *Phys. Rev. D* **70** (2004) 073015, [[hep-ph/0405191](#)].
- [51] A. Arbuzov et al., *One-loop corrections to the Drell-Yan process in SANC. I. The Charged current case*, *Eur. Phys. J. C* **46** (2006) 407–412, [[hep-ph/0506110](#)]. [Erratum: *Eur.Phys.J.C* 50, 505 (2007)].
- [52] C. Carloni Calame, G. Montagna, O. Nicrosini, and A. Vicini, *Precision electroweak calculation of the charged current Drell-Yan process*, *JHEP* **12** (2006) 016, [[hep-ph/0609170](#)].
- [53] V. Zykunov, *Weak radiative corrections to Drell-Yan process for large invariant mass of di-lepton pair*, *Phys. Rev. D* **75** (2007) 073019, [[hep-ph/0509315](#)].
- [54] C. Carloni Calame, G. Montagna, O. Nicrosini, and A. Vicini, *Precision electroweak calculation of the production of a high transverse-momentum lepton pair at hadron colliders*, *JHEP* **10** (2007) 109, [[arXiv:0710.1722](#)].
- [55] A. Arbuzov, et al., *One-loop corrections to the Drell-Yan process in SANC. (II). The Neutral current case*, *Eur. Phys. J. C* **54** (2008) 451–460, [[arXiv:0711.0625](#)].
- [56] S. Brensing, S. Dittmaier, M. Krämer, and A. Mück, *Radiative corrections to  $W^-$  boson hadroproduction: Higher-order electroweak and supersymmetric effects*, *Phys. Rev. D* **77** (2008) 073006, [[arXiv:0710.3309](#)].
- [57] S. Dittmaier and M. Huber, *Radiative corrections to the neutral-current Drell-Yan process in the Standard Model and its minimal supersymmetric extension*, *JHEP* **01** (2010) 060, [[arXiv:0911.2329](#)].
- [58] L. Barze, et al., *Neutral current Drell-Yan with combined QCD and electroweak corrections in the POWHEG BOX*, *Eur. Phys. J. C* **73** (2013) 2474, [[arXiv:1302.4606](#)].
- [59] R. Boughezal, Y. Li, and F. Petriello, *Disentangling radiative corrections using the high-mass Drell-Yan process at the LHC*, *Phys. Rev. D* **89** (2014) 034030, [[arXiv:1312.3972](#)].
- [60] L. Cieri, G. Ferrera, and G. F. R. Sborlini, *Combining QED and QCD transverse-momentum resummation for Z boson production at hadron colliders*, *JHEP* **08** (2018) 165, [[arXiv:1805.11948](#)].



- [61] A. Autieri, L. Cieri, G. Ferrera, and G. F. R. Sborlini, *Combining QED and QCD transverse-momentum resummation for W and Z boson production at hadron colliders*, *JHEP* **07** (2023) 104, [[arXiv:2302.05403](#)].
- [62] W. Placzek and S. Jadach, *Multiphoton radiation in leptonic W boson decays*, *Eur. Phys. J. C* **29** (2003) 325–339, [[hep-ph/0302065](#)].
- [63] C. Carloni Calame, G. Montagna, O. Nicrosini, and M. Treccani, *Higher order QED corrections to W boson mass determination at hadron colliders*, *Phys. Rev. D* **69** (2004) 037301, [[hep-ph/0303102](#)].
- [64] S. Dittmaier, A. Huss, and C. Schwinn, *Mixed QCD-electroweak  $O(\alpha_s\alpha)$  corrections to Drell-Yan processes in the resonance region: pole approximation and non-factorizable corrections*, *Nucl. Phys. B* **885** (2014) 318–372, [[arXiv:1403.3216](#)].
- [65] S. Dittmaier, A. Huss, and C. Schwinn, *Dominant mixed QCD-electroweak  $O(\alpha_s\alpha)$  corrections to Drell-Yan processes in the resonance region*, *Nucl. Phys. B* **904** (2016) 216–252, [[arXiv:1511.08016](#)].
- [66] A. Denner and S. Dittmaier, *Electroweak Radiative Corrections for Collider Physics*, *Phys. Rept.* **864** (2020) 1–163, [[arXiv:1912.06823](#)].
- [67] A. Behring et al., *Mixed QCD-electroweak corrections to W-boson production in hadron collisions*, *Phys. Rev. D* **103** (2021) 013008, [[arXiv:2009.10386](#)].
- [68] R. Bonciani, F. Buccioni, R. Mondini, and A. Vicini, *Double-real corrections at  $\mathcal{O}(\alpha\alpha_s)$  to single gauge boson production*, *Eur. Phys. J. C* **77** (2017) 187, [[arXiv:1611.00645](#)].
- [69] D. de Florian, M. Der, and I. Fabre, *QCD $\oplus$ QED NNLO corrections to Drell-Yan production*, *Phys. Rev. D* **98** (2018) 094008, [[arXiv:1805.12214](#)].
- [70] M. Delto, M. Jaquier, K. Melnikov, and R. Röntsch, *Mixed QCD $\otimes$ QED corrections to on-shell Z boson production at the LHC*, *JHEP* **01** (2020) 043, [[arXiv:1909.08428](#)].
- [71] R. Bonciani et al., *NNLO QCD $\times$ EW corrections to Z production in the  $q\bar{q}$  channel*, *Phys. Rev. D* **101** (2020) 031301, [[arXiv:1911.06200](#)].
- [72] L. Cieri, D. de Florian, M. Der, and J. Mazzitelli, *Mixed QCD $\otimes$ QED corrections to exclusive Drell Yan production using the  $q_T$ -subtraction method*, [arXiv:2005.01315](#).
- [73] F. Buccioni, et al., *Mixed QCD-electroweak corrections to on-shell Z production at the LHC*, *Phys. Lett. B* **811** (2020) 135969, [[arXiv:2005.10221](#)].
- [74] R. Bonciani, F. Buccioni, N. Rana, and A. Vicini, *Next-to-Next-to-Leading Order Mixed QCD-Electroweak Corrections to on-Shell Z Production*, *Phys. Rev. Lett.* **125** (2020) 232004, [[arXiv:2007.06518](#)].

- [75] R. Bonciani, F. Buccioni, N. Rana, and A. Vicini, *On-shell Z boson production at hadron colliders through  $O(\alpha\alpha_s)$* , *JHEP* **02** (2022) 095, [[arXiv:2111.12694](#)].
- [76] S. Dittmaier, T. Schmidt, and J. Schwarz, *Mixed NNLO QCD $\times$ electroweak corrections of  $O(N_f\alpha_s\alpha)$  to single-W/Z production at the LHC*, *JHEP* **12** (2020) 201, [[arXiv:2009.02229](#)].
- [77] L. Buonocore, M. Grazzini, S. Kallweit, C. Savoini, and F. Tramontano, *Mixed QCD-EW corrections to  $pp\rightarrow\ell\nu_\ell+X$  at the LHC*, *Phys. Rev. D* **103** (2021) 114012, [[arXiv:2102.12539](#)].
- [78] R. Bonciani, et al., *Mixed Strong-Electroweak Corrections to the Drell-Yan Process*, *Phys. Rev. Lett.* **128** (2022) 012002, [[arXiv:2106.11953](#)].
- [79] T. Armadillo, R. Bonciani, S. Devoto, N. Rana, and A. Vicini, *Two-loop mixed QCD-EW corrections to neutral current Drell-Yan*, *JHEP* **05** (2022) 072, [[arXiv:2201.01754](#)].
- [80] F. Buccioni, et al., *Mixed QCD-electroweak corrections to dilepton production at the LHC in the high invariant mass region*, *JHEP* **06** (2022) 022, [[arXiv:2203.11237](#)].
- [81] A. Kotikov, J. H. Kühn, and O. Veretin, *Two-Loop Formfactors in Theories with Mass Gap and Z-Boson Production*, *Nucl. Phys. B* **788** (2008) 47–62, [[hep-ph/0703013](#)].
- [82] A. Daleo, T. Gehrmann, and D. Maitre, *Antenna subtraction with hadronic initial states*, *JHEP* **04** (2007) 016, [[hep-ph/0612257](#)].
- [83] S. Catani and M. Seymour, *A General algorithm for calculating jet cross-sections in NLO QCD*, *Nucl. Phys. B* **485** (1997) 291–419, [[hep-ph/9605323](#)]. [Erratum: *Nucl.Phys.B* 510, 503–504 (1998)].
- [84] A. Gehrmann-De Ridder, T. Gehrmann, and E. W. N. Glover, *Antenna subtraction at NNLO*, *JHEP* **09** (2005) 056, [[hep-ph/0505111](#)].
- [85] J. Currie, E. W. N. Glover, and S. Wells, *Infrared structure at NNLO using antenna subtraction*, *JHEP* **04** (2013) 066, [[arXiv:1301.4693](#)].
- [86] A. Daleo, A. Gehrmann-De Ridder, T. Gehrmann, and G. Luisoni, *Antenna subtraction at NNLO with hadronic initial states: initial-final configurations*, *JHEP* **01** (2010) 118, [[arXiv:0912.0374](#)].
- [87] T. Gehrmann and P. Monni, *Antenna subtraction at NNLO with hadronic initial states: real-virtual initial-initial configurations*, *JHEP* **12** (2011) 049, [[arXiv:1107.4037](#)].
- [88] A. Gehrmann-De Ridder, T. Gehrmann, and M. Ritzmann, *Antenna subtraction at NNLO with hadronic initial states: double real initial-initial configurations*, *JHEP* **10** (2012) 047, [[arXiv:1207.5779](#)].

- [89] J. Kublbeck, M. Böhm, and A. Denner, *Feyn Arts: Computer Algebraic Generation of Feynman Graphs and Amplitudes*, *Comput. Phys. Commun.* **60** (1990) 165–180.
- [90] P. Maierhöfer, J. Usovitsch, and P. Uwer, *Kira—A Feynman integral reduction program*, *Comput. Phys. Commun.* **230** (2018) 99–112, [[arXiv:1705.05610](#)].
- [91] P. Maierhöfer and J. Usovitsch, *Kira 1.2 Release Notes*, [arXiv:1812.01491](#).
- [92] J. M. Henn, *Multiloop integrals in dimensional regularization made simple*, *Phys. Rev. Lett.* **110** (2013) 251601, [[arXiv:1304.1806](#)].
- [93] J. M. Henn, *Lectures on differential equations for Feynman integrals*, *J. Phys. A* **48** (2015) 153001, [[arXiv:1412.2296](#)].
- [94] A. B. Goncharov, *Multiple polylogarithms, cyclotomy and modular complexes*, *Math. Res. Lett.* **5** (1998) 497–516, [[arXiv:1105.2076](#)].
- [95] A. B. Goncharov, M. Spradlin, C. Vergu, and A. Volovich, *Classical Polylogarithms for Amplitudes and Wilson Loops*, *Phys. Rev. Lett.* **105** (2010) 151605, [[arXiv:1006.5703](#)].
- [96] S. Buehler and C. Duhr, *CHAPLIN - Complex Harmonic Polylogarithms in Fortran*, *Comput. Phys. Commun.* **185** (2014) 2703–2713, [[arXiv:1106.5739](#)].
- [97] L. Naterop, A. Signer, and Y. Ulrich, *handyG —Rapid numerical evaluation of generalised polylogarithms in Fortran*, *Comput. Phys. Commun.* **253** (2020) 107165, [[arXiv:1909.01656](#)].
- [98] A. Gehrmann-De Ridder, T. Gehrmann, and E. W. N. Glover, *Infrared structure of  $e^+e^- \rightarrow 2$  jets at NNLO*, *Nucl. Phys. B* **691** (2004) 195–222, [[hep-ph/0403057](#)].
- [99] T. Gehrmann, T. Huber, and D. Maitre, *Two-loop quark and gluon form-factors in dimensional regularisation*, *Phys. Lett. B* **622** (2005) 295–302, [[hep-ph/0507061](#)].
- [100] A. Denner, S. Dittmaier, T. Kasprzik, and A. Muck, *Electroweak corrections to dilepton + jet production at hadron colliders*, *JHEP* **06** (2011) 069, [[arXiv:1103.0914](#)].
- [101] A. Gehrmann-De Ridder, et al., *Precision phenomenology with fiducial cross sections in the triple-differential Drell-Yan process*, *JHEP* **05** (2023) 002, [[arXiv:2301.11827](#)].
- [102] T. Hahn, *Generating Feynman diagrams and amplitudes with FeynArts 3*, *Comput. Phys. Commun.* **140** (2001) 418–431, [[hep-ph/0012260](#)].
- [103] T. Hahn and M. Perez-Victoria, *Automated one-loop calculations in four and  $d$  dimensions*, *Computer Physics Communications* **118** (1999) 153–165.

- [104] A. Denner, S. Dittmaier, and L. Hofer, *Collier: a fortran-based Complex One-Loop Library in Extended Regularizations*, *Comput. Phys. Commun.* **212** (2017) 220–238, [[arXiv:1604.06792](#)].
- [105] S. Dittmaier, *Weyl-van der Waerden formalism for helicity amplitudes of massive particles*, *Phys. Rev. D* **59** (1998) 016007, [[hep-ph/9805445](#)].
- [106] **Particle Data Group** Collaboration, J. Beringer et al., *Review of Particle Physics (RPP)*, *Phys. Rev. D* **86** (2012) 010001.
- [107] **NNPDF** Collaboration, V. Bertone, S. Carrazza, N. P. Hartland, and J. Rojo, *Illuminating the photon content of the proton within a global PDF analysis*, *SciPost Phys.* **5** (2018) 008, [[arXiv:1712.07053](#)].
- [108] A. Denner, S. Dittmaier, M. Roth, and L. Wieders, *Electroweak corrections to charged-current  $e^+e^- \rightarrow 4$  fermion processes: Technical details and further results*, *Nucl. Phys. B* **724** (2005) 247–294, [[hep-ph/0505042](#)]. [Erratum: *Nucl.Phys.B* 854, 504–507 (2012)].
- [109] M. Rubin, G. P. Salam, and S. Sapeta, *Giant QCD K-factors beyond NLO*, *JHEP* **09** (2010) 084, [[arXiv:1006.2144](#)].
- [110] E. A. Kuraev and V. S. Fadin, *On Radiative Corrections to  $e^+e^-$  Single Photon Annihilation at High-Energy*, *Sov. J. Nucl. Phys.* **41** (1985) 466–472.
- [111] O. Nicrosini and L. Trentadue, *Soft Photons and Second Order Radiative Corrections to  $e^+e^- \rightarrow Z^0$* , *Phys. Lett. B* **196** (1987) 551.
- [112] O. Nicrosini and L. Trentadue, *Second order electromagnetic radiative corrections to  $e^+e^- \rightarrow \gamma^*$ ,  $Z^0 \rightarrow \mu^+\mu^-$* , *Z. Phys. C* **39** (1988) 479.
- [113] F. A. Berends, W. L. van Neerven, and G. J. H. Burgers, *Higher Order Radiative Corrections at LEP Energies*, *Nucl. Phys. B* **297** (1988) 429. [Erratum: *Nucl.Phys.B* 304, 921 (1988)].
- [114] A. B. Arbuzov, *Nonsinglet splitting functions in QED*, *Phys. Lett. B* **470** (1999) 252–258, [[hep-ph/9908361](#)].
- [115] Blümlein, Johannes and Kawamura, Hiroyuki, *Universal higher order singlet QED corrections to unpolarized lepton scattering*, *Eur. Phys. J. C* **51** (2007) 317–333, [[hep-ph/0701019](#)].
- [116] Blümlein, Johannes and De Freitas, Abilio and van Neerven, Wilhelmus, *Two-loop QED Operator Matrix Elements with Massive External Fermion Lines*, *Nucl. Phys. B* **855** (2012) 508–569, [[arXiv:1107.4638](#)].
- [117] J. Blümlein, A. De Freitas, C. Raab, and K. Schönwald, *The  $O(\alpha^2)$  initial state QED corrections to  $e^+e^- \rightarrow \gamma^*/Z_0^*$* , *Nucl. Phys. B* **956** (2020) 115055, [[arXiv:2003.14289](#)].

- [118] E. Barberio and Z. Was, *PHOTOS: A Universal Monte Carlo for QED radiative corrections. Version 2.0*, *Comput. Phys. Commun.* **79** (1994) 291–308.
- [119] J. C. Collins and D. E. Soper, *Angular Distribution of Dileptons in High-Energy Hadron Collisions*, *Phys. Rev. D* **16** (1977) 2219.
- [120] CMS Collaboration, V. Khachatryan et al., *Forward–backward asymmetry of Drell–Yan lepton pairs in pp collisions at  $\sqrt{s} = 8$  TeV*, *Eur. Phys. J. C* **76** (2016) 325, [[arXiv:1601.04768](#)].
- [121] S. Laporta, *High precision calculation of multiloop Feynman integrals by difference equations*, *Int. J. Mod. Phys. A* **15** (2000) 5087–5159, [[hep-ph/0102033](#)].
- [122] J. Klappert, F. Lange, P. Maierhöfer, and J. Usovitsch, *Integral reduction with Kira 2.0 and finite field methods*, *Comput. Phys. Commun.* **266** (2021) 108024, [[arXiv:2008.06494](#)].